NUMERICAL ANALYSIS OF BOND BETWEEN STEEL AND CONCRETE UNDER ELEVATED TEMPERATURES

Author: Asier Gil Sedano

Examiner: Akanshu Sharma

Supervisor: Josipa Bošnjak

15/09/2018

STUTTGART UNIVERSITY

Index

1 Introduction

1.1 Background and context

The concrete structures behavior for high temperatures has been an object of study during the recent years and even if huge improvements have been made in this area, there are still certain characteristics and properties that should be researched. This changes in the characteristics and the high temperature behavior of the structures has been considered in the construction codes but the bond behavior under elevated temperatures is a field in which there is not much available literature and it is no guidance is proposed in the codes. Furthermore, the unique properties of the concrete and the vast quantity of factors that can affect the behavior make it a difficult subject of study. Because of this reason, the numerical analysis for the concrete is a very effective way to understand the behavior of the concrete and the different elements involved but needs to be validated by experimental data.

The concrete behavior depending on the temperature has been relatively well defined by the several researchers that have been studying this degradation of the properties and all the studies converge to more or less similar results. In general, thermal exposure leads to a change in physical as well as mechanical properties which should be considered in all the studies related to this matter.

Among all the changes of the concrete properties depending on the temperature, the severe reduction on the tensile strength, and the reduction of the compressive strength are the most remarkable properties. That reduction will mostly depend on the peak temperature during the heating. Other properties such as the fracture energy also vary with the temperature. Because of this reduction of the different properties, it is important to measure how the degradation of the concrete affects the bond because the bearing capacity and the bond performance can be heavily decreased if the bond strength is reduced.

When it comes to analyze the behavior of reinforced concrete, the bond between the steel and concrete needs to be well defined, and for high temperatures this temperature dependency needs to be properly evaluated. This bond study involves all the different bond failure modes which are splitting and pull-out failure and how the different failure mechanisms depend on different properties and how the temperature behavior varies from one to the other. Another important characteristic that should be defined is the possibility of a change from pure bond failure to splitting failure due to this change in the concrete properties. For that is important to measure the bond degradation and determine the main influencing factors. Diederichs, U & Schneider, U. (1981) studied the concrete-steel bond behavior at high temperatures, where different pull-out failure tests were performed for different temperatures and loads. The results indicated that the bond strength at high temperatures, were greater than the reduction of the compressive strength. Morley and Royles (1983) tested the behavior of the bond strength for different load and heating combinations. The results also indicated that the strength after the cooling is lower than

it is at high temperatures, which is very important to determine the possible serviceability after the fire.

However, these studies only refer to the pure bond failure and do not consider how due to the reduction of the tensile strength the splitting could be more likely to happen at high temperatures while for service temperatures would not. This is a critical factor that should be studied because it will highly influence in the behavior of loaded beams for example and many other structural elements in which the reinforcement is used. Bošnjak J., Sharma A. & Bessert S. (2017) studied the effect on the bond strength after cooling for different rebar positions, reporting that the degradation of the strength against the splitting failure, decreases more closely linear to the degradation of the tensile strength of the concrete. They also reported that the presence of cracks significantly influences the residual bond capacity, especially for relatively small concrete covers.

The heating rate is also a very critical value that needs to be considered. In order to avoid the effects of the high temperature gradients on the thermal stresses and create cracks that would reduce the concrete strength, a low heating should be applied to the specimens. In this study the heating rate applied was 2ºC/minute, enough to fulfill this purpose.

Other aspects such as the effect of the relative rib area, aggregate type, concrete strength, concrete cover and the position of the rebar within the reinforced concrete have been an object of study demonstrating that the usable bond strength of a rebar is limited by the splitting failure, yielding at lower loads than the ones for pure bond failure (not splitting).

It is very important to consider all the different factors involved and how the different phenomena, such as the change of the properties depending on the temperature that lead to different failure modes affect to the result. This involves two different types of analysis that can be performed. First, we have the thermomechanical, where only the different physical properties and how they vary depending on the temperature are considered. We secondly have the thermo-hygro-mechanical analysis, where all the different properties that are involved in the concrete behavior are considered such as moisture, temperature, pore pressure and concrete hydration. This second analysis is clearly more complete but also more complex and hence not suitable for investigation of bond behavior.

As the costs and the complexity of testing for high temperatures is relatively high, a numerical analysis of the fire performance of the structures gives a very high flexibility for the study of some properties such as the bond performance for high temperatures. One of the main prerequisites for the numerical investigation is the validation of the modelling approach using experimental results. In the current work the results of the tests for bond performance at high temperatures study from Bošnjak J., Sharma A. & Bessert S. (2017) will be contrasted. The same specimens are modelled to compare the crack pattern and the bond strength after fire for validation, after that a parametric study is done for different bond lengths and rebar positions.

The numerical analysis using finite elements is an adequate approach for this type of analysis. In this case, the study is performed using the software MASA based on the microplane model and developed by Prof. J. Ozbolt (University of Stuttgart).

1.2 Objectives

The objectives of this thesis are:

1. Validate the models comparing with results obtained by experimental pull-out failure tests.
2. Study the relationship between the residual bond strength and the temperature
3. Analyze the influence of the bond length on the bond performance and different types of failure.
4. Analyze the effect of concrete cover and the different bar positions for determining the pull-out failure.
5. Test the effect of the different bond lengths and the development of the stresses through the bond length and the effect of the temperature in this development length.

2 Literature review

2.1 Concrete-Steel bond

Since the aim of this thesis is to analyze the influence of the temperature in the concrete-steel bond, a good understanding of the bond theory is required.

2.1.1 General bond concepts and failure mechanisms

The bond between steel and concrete makes the reinforced concrete behave as a composite material. For this composite material behavior to happen, a proper force transmission between the steel and the concrete needs to be achieved. This force can only be transferred though the bond. The bond stress is defined as the shear force per unit area of bar surface being given by the following equation:

$$u = \frac{q}{\sum o} = \frac{\Delta f_s A_b}{\sum o} = \frac{d_b}{4}\Delta f_s \tag{2.1}$$

Being q the change of bar force over unit length, $\sum o$ the nominal surface area of a bar of unit length, d_b the nominal diameter of the bar, Δf_s the change of steel stress over unit length and A_b the area of the bar. When it comes to plain bars the bond strength is very much dependent on many factors and force transmission is not very high, but the ribbed bars have greatly improved this aspect.

The bond between the concrete and the steel is created by the ribs of the reinforcement and the stresses that transmit the force between the two different elements. These stresses are shown in the Figure 1.

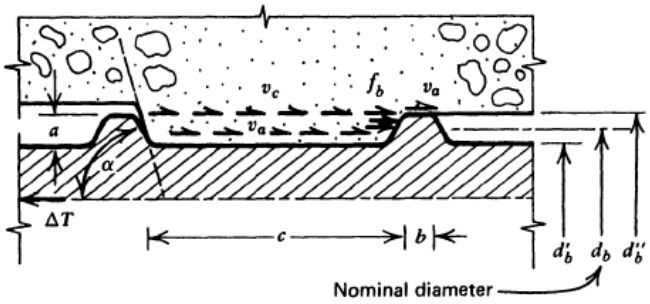

Figure 1. Stresses transmitted from the reinforcement to the concrete.

The bond stress in reinforced concrete can be a consequence of two effects, the variation of the bending moment along a beam or a structural element c, or from the anchorage of bars. There is a concept called the development length that indicates how long the bond distance must be to be able to transmit a specific force from the bar to the concrete or vice versa. Considering the following equation:

$$T = A_b f_s = u\, \Sigma o\, l_d \tag{2.2}$$

We can deduce that the development length will be determined by:

$$l_d = \frac{d_b}{4u} f_s \tag{2.3}$$

Being d_b the nominal diameter, f_s the steel stress and u the shear force per unit area. The values of the anchorage bond stresses are usually set by the codes so the equation (2.3) can be used to calculate the development length.

Theoretically for flexural reinforcement, the tension force T must vary at the same rate as the variation of the bending moment. But since there is a presence of cracks in the concrete, even when the shear force is zero (constant bending moment) there is bond stress, so the bond variation for bending elements is not easy to define. The codes give also secure values for this situation of bond stress variation rate.

These stresses, according to Park and Paulay (1975) can be divided in three different stresses:

1. The shear stress v_a developed through the adhesion to the concrete along the surface of the bar.

2. The bearing stresses f_b that are created by the facing between the rib and the concrete.

3. Shear stresses v_c that are acting on the cylindrical concrete surface between adjacent ribs.

The relation between these stresses and the force to be transferred to the concrete can be obtained using equilibrium leading to the following equation:

$$\Delta T = \pi d_b'(b + c)v_a + \pi \frac{d_b''^2 - d_b'^2}{4} f_b \approx \pi d_b'' c v_c \tag{2.4}$$

As the load increases, the adhesion created by v_a breaks and a residual very small value remains, which can be neglected for simplicity reasons, meaning that the only stresses contributing to the bond stress are the v_c and f_b. Using geometrical relations from Figure 1 the following relation is obtained:

$$v_c \approx \frac{a}{c} f_b \tag{2.5}$$

Rehm (1961) indicated that the failure mechanism depends very much on the *a/c* relationship (being *a* the rib length and *c* the distance between ribs), concluding that 0.065 was the transient value from a break mechanism to the other. Two different bond failure mechanisms can be differentiated, the pure bond failure, occurring when the ribs are too closely spaced and the splitting failure, generated when the concrete is crushed and creates a wedge around the rib even if in some cases also the pull-out failure can happen for this type of configuration. These failure mechanisms are illustrated in the Figure 2.

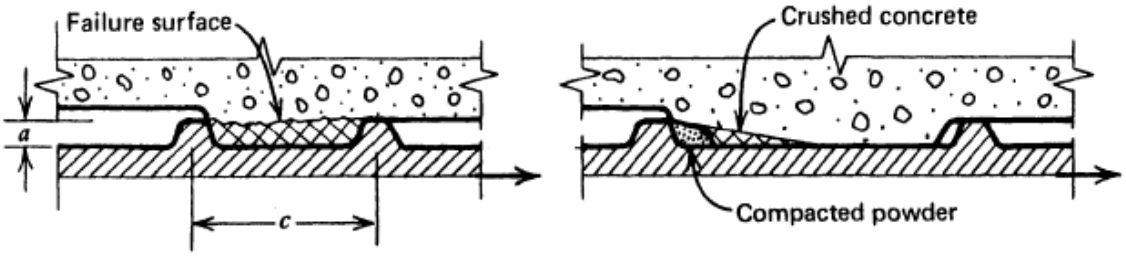

Figure 2. Failure mechanisms at the ribs for deformed bars. a/c >0.15 (left) a/c <0.1 (right).

When the rebar is transmitting high loads, a major crack in concrete occurs, the crack surrounding concrete deforms tending to separate the concrete from the rebar as shown in the Figure 3. When this effect happens, the rebar transmits all the force trough the bearing of the rib creating tensile stresses that lead to longitudinal splitting cracks.

The splitting can also occur because of other reasons. As seen in the Figure 2 (right), when the bond reaches its ultimate load, the compacted concrete powder, extended in front of the rib forms a wedge pushing the concrete far away from the bar. This effect creates circumferential stresses that may also lead to splitting failure. This effect is increased when there are more rebars in a lap splice for example, where this splitting crack can be more likely to happen by the combination of this same effect in different rebars.

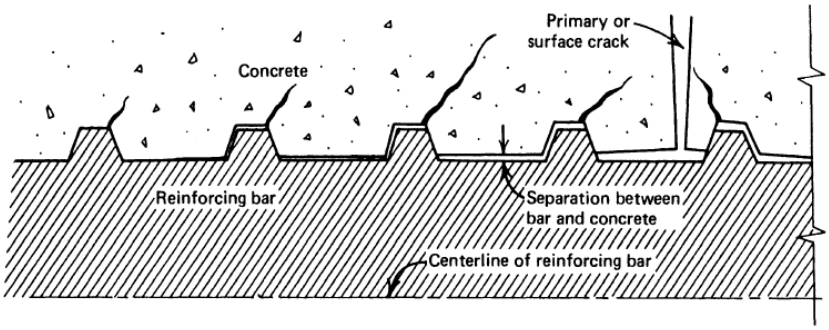

Figure 3. Bond development in the major crack surroundings.

This splitting failure is directly influenced by the cover of concrete, as the cover increases, the splitting is less likely to happen and more bond strength will be able to be performed until the failure. According to Ferguson and Thompson (1965) this relationship between the concrete and the bond strength is not directly proportional to the concrete cover. They also indicate that a high cover loses effectiveness as the bond length is increased. Indeed, the larger the bar bond length used, the easier it will be the splitting to happen. Ideally, the concrete cover should be enough to avoid this splitting failure and make the bond failure be a pure bond failure instead of splitting. In a beam when more than one reinforcement rebar is used and they are closely spaced, the splitting is more likely to happen.

When enough concrete cover is used, the pure bond strength can be developed and therefore, no splitting happens making more efficient use of this bond strength. When the

conditions do not allow the bond strength to be developed, the splitting is happening. This transition between the pure bond failure to the splitting failure depends on different factors such as the concrete cover, concrete strength, the presence of transversal reinforcement, diameter of the bar… For example, by increasing the cover, the splitting will be less likely to occur, or the transversal reinforcement will also make the splitting more difficult to happen. The bond stress for different failure modes is shown in the Figure 6 according to the fib Model Code 2010.

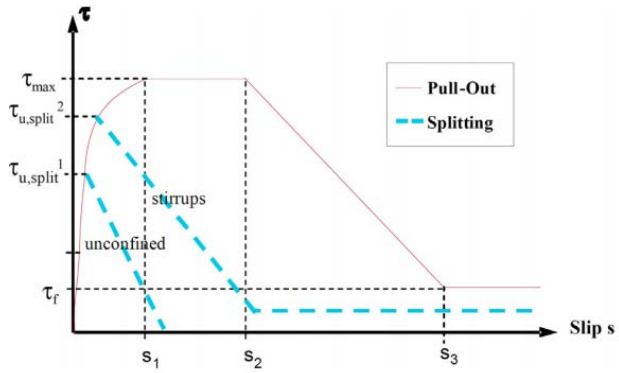

Figure 4. Bond development for different failure modes and conditions (fib Model Code 2010).

The study of the bond stress-slip relationship for pull-out failure is recommended by the fib Model Code 2010 to be studied analytically by using the expression (2.6) where η is the factor to consider bond conditions, f_{cm} is the mean cylinder concrete compressive strength in MPa, ϕ is the diameter of the anchored bar in mm, c_{min}/c_{max} is the ratio between the minimum and maximum concrete cover and k_m, k_{tr} are the factors to consider the influence of the transverse reinforcement.

$$\tau_{bu,split} = \eta_2 \, 6.5 \left(\frac{f_{cm}}{25}\right)^{0.25} \left(\frac{25}{\phi}\right)^{0.20} \left[\left(\frac{c_{min}}{\phi}\right)^{0.23} \left(\frac{c_{max}}{c_{min}}\right)^{0.1} + k_m K_{tr}\right] \tag{2.6}$$

If the confinement by the usage of transverse compression is applied, the concrete will be able to hold a higher bond stress before the splitting happens. This is usually done by the usage of stirrups. Even if the stirrups will not avoid the splitting, they can reduce how much the cracks are opened and lead to a more ductile type of bond failure occurs.

2.1.2 Bond development length

As it happens in all the composite materials, the stresses are not uniform for the whole length in which the forces are transmitted. As the force is being transmitted, the stresses in the rebar are not uniform. Because of this reason, the stresses along the length are not constant and there is usually a concentration of stresses in the front part of the bond, leading to a crack and failing and not permitting the whole bond strength to be developed.

For small bond lengths this effect is not very influential and the loss in the bond strength is not very significant, but since in the reality long bond lengths are used there is a need to determine and quantify this effect. The qualitative stress profile can be as shown in the Figure 5.

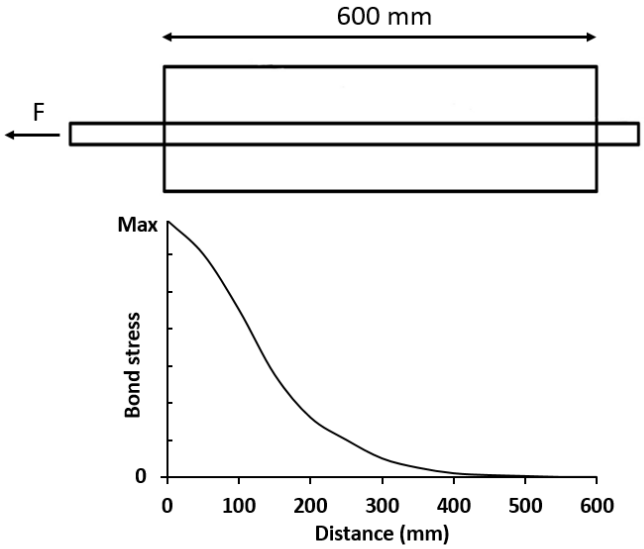

Figure 5. Bond stress development along the bond distance for a pull-out test according to Rashedul et al. (2014).

It can be observed how for high bond distances, the decrease on the bond stress can be drastically decreased. It can also be observed how for values higher than 400 mm almost no bond load is transmitted.

The fib Model Code 2010 proposes an approach in which a constant stress along the bond distance is assumed, but a reduction factor is considered to decrease the bond total capacity depending on the bond length. Generally, it is accepted to assume that the bond stress is constant for bond lengths up to 5 times the diameter.

2.1.3 High temperatures

As explained before, the splitting is a type of bond failure that reduces the bond strength by a failure in concrete. This failure is mainly because of the creation of cracks due to tensile stresses. As explained before, the tensile strength of the concrete is reduced significantly as there is an increase on the temperature. Consequently, it can be expected that a reduction in the tensile strength leads to a reduction of the bond strength.

The reduction on the bond strength between the steel and concrete for high temperatures was studied by numerous researchers, such as Diedrich and Schneider (1982). Diederich and Schneider reported that the bond strength depends not only in the temperature but also in the test procedure and the type of the bar (smooth or ribbed). They also reported that the bond strength loss is proportional to the reduction of the compressive strength for that temperature.

Morley and Royles performed different tests for the same specimens:

1. They bar was pulled during the heating to a certain temperature and then loaded to failure while hot.

2. Exactly equal to (1) and then loaded to failure after being cooled.

3. No stress applied while heating to a specific temperature and then loaded to failure while hot.

4. Equal to (3) and then loaded to failure after cooling.

The results for ribbed bars showed that for temperatures from 20°C to 300°C even though there was relatively low decrease on the strength, the curves maintained the same shape. For temperatures higher than 300°C the shape of the curves changed more than for temperatures below this value. These results can be observed in the Figure 6.

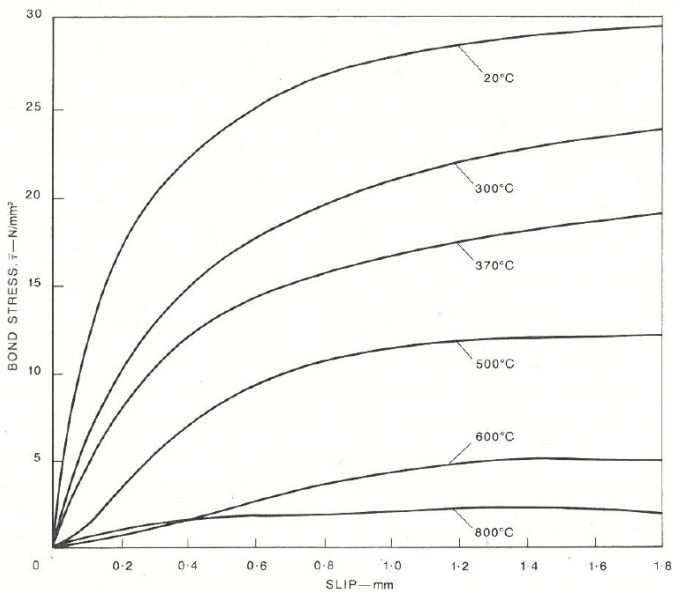

Figure 6. Bond-stress-slip relationship of ribbed bars at different temperatures tested while hot.

For the testing of the specimens that were stressed while hot. It is important to remark that the results were also affected by the expansion of the different elements composing the specimen. As it can be seen in the Figure 7 this starts affecting even for the non-tested specimens from temperatures higher than 400°C. In the same figure it can be observed the reduction on the strength for different temperatures.

The heating rates for all these tests, measured in the outer surface was of 1K/min.

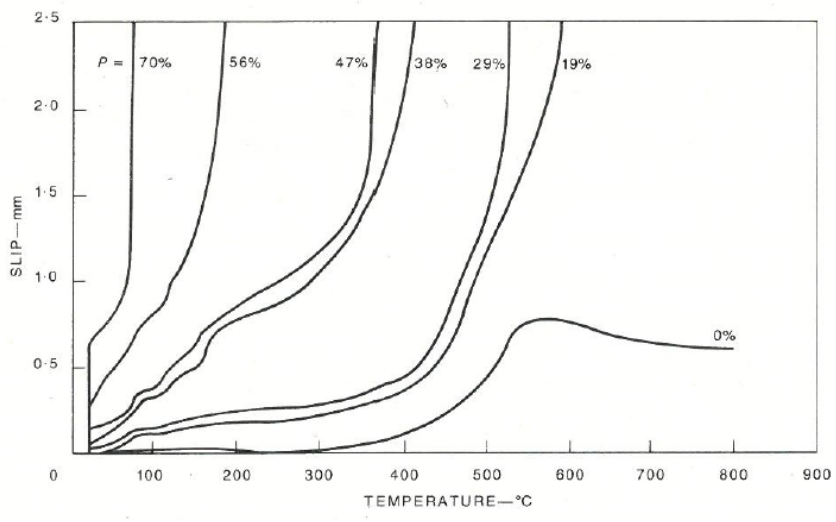

Figure 7. Temperature-slip behavior for ribbed bars loaded while heating.When it comes to evaluate the bond degradation depending on the temperature, several studies are available. Measured for different rebar diameters and different types of concrete but as observed in the ------ they all converge to the same orientation. It is important to remark that all these results are for the case of the pure bond failure, which means that the splitting failure is not being considered.

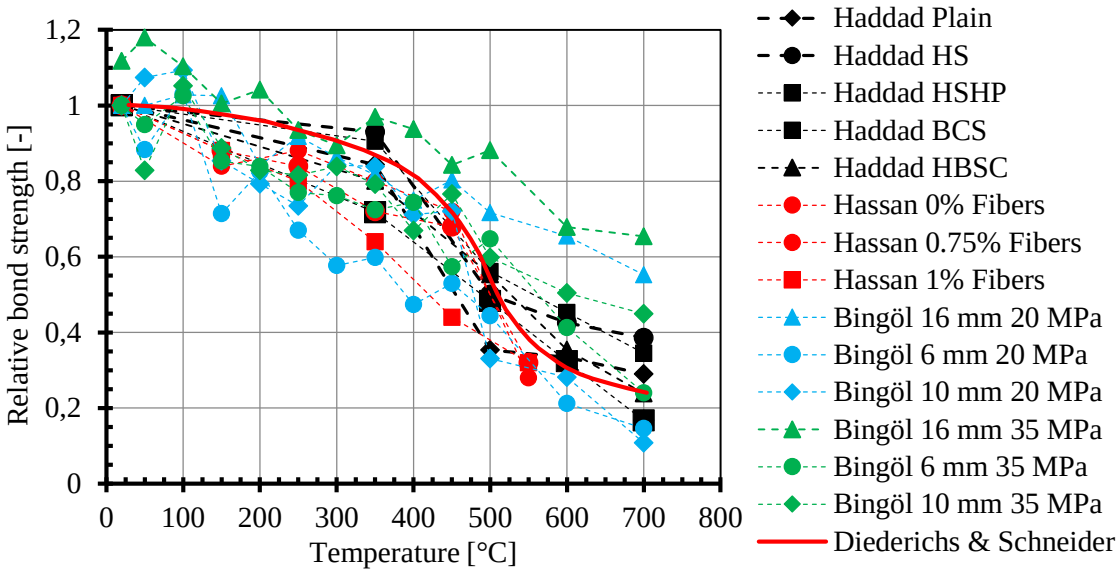

Figure 8. Previous studies for bond degradation depending on the temperature.

2.2 Effect of the high temperatures on the concrete

2.2.1 General Aspects

For the study of the concrete it is important to know what are the different processes that are affecting the concrete behavior at elevated temperatures During heating, concrete undergoes different stages which are important to understand the behavior (Bazant and Kaplan 1996):

1. The evaporable water is discharged from hardened cement paste and aggregate at temperatures about 100°C.

2. The dehydration of the cement gel starts with temperatures above 100 degrees Celsius.

3. The $Ca(OH)_2$ is decomposed in the cement paste. This decomposition is more pronounced for temperatures above 500 degrees Celsius.

4. The α-quartz of the aggregates is transformed to β-quartz at temperatures about 570 degrees Celsius for quartzite and basalt aggregate concretes.

5. The calcium silicate hydrates in the cement paste start to decompose at temperatures about 700 degrees Celsius.

6. The calcium carbonate in the limestone aggregate concrete decarbonate for temperatures of 800 degrees Celsius.

7. The cement paste and aggregate melt at temperatures about 1150-1200 degrees Celsius.

One of the most important effects of the high temperatures on the concrete is the thermal expansion, which for high temperatures is a very important factor to consider, especially for high heating ratios. The concrete expansion can lead to high tensile stresses in concrete. This differences in the concrete expansion for high temperature gradients, can lead to cracks influencing on the damage of the concrete after fire and reducing the strength. As described by William et al. (2009) another critical factor for the concrete strength loss is the incompatibility between the cement paste and the aggregate that may cause a large mismatch between the deformation the components. Furthermore, steel concrete expansion is relatively similar only for temperatures below 400°C, with a more pronounced difference at higher temperatures.

As reported by Schneider (1982) the concrete strength loss is higher after the cooling than it is while it is hot which is important to remark and consider for the testing. When cooled, the cracks cannot fully close and therefore the tensile strength is decreased even more.

Also the mismatch in the thermal expansions between the aggregates and the matrix also has a big influence and when the cooling happens and extra damage is introduced in the concrete leading to a greater reduction. All the effects mentioned before will be more detailed in the following chapters.

2.2.2 Compressive strength

Numerous studies have reported the variability of the concrete strength depending on the temperature (Morita 1992, Khoury 1999, Felicetti 1996, Phan & Carino 2001, Schneider 1992) and reported the variability depending on the type of concrete and aggregate, see Figure 1. Majority of the researchers found that there is only a low decrease of the compressive strength for temperatures below 300 degrees Celsius.

It has also been reported and specified in ACI 216 that for high temperatures the concrete gains strength for temperatures between 100-200 degrees Celsius and then decreased for higher temperatures. As reported by Lublóy et al. (2004) this increase on the strength can be about a 5-10%, while tested cold there is indeed a decrease on the strength for these temperatures which demonstrates that the behavior of the concrete depends very much on the testing conditions. For concrete strength after cooling the relative compressive strength follows the curve shown in Figure 9.

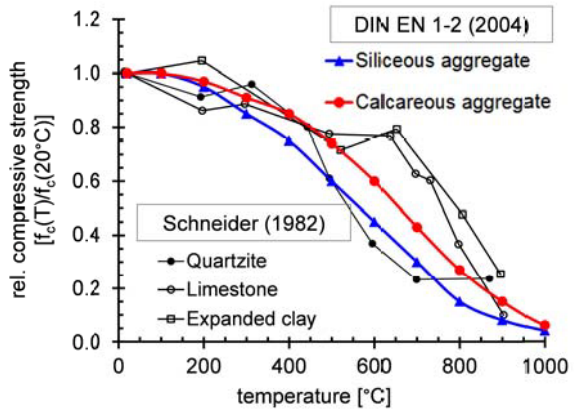

Figure 9. Concrete relative strength after cooling for different aggregates.

This behavior is modelled in the numerical analysis by the variation of the concrete strength depending on the temperature. As indicated by Periskic (2009) the variation of the concrete strength in the thermo-mechanical model for concrete used in this study follows the curve indicated in the Figure 10.

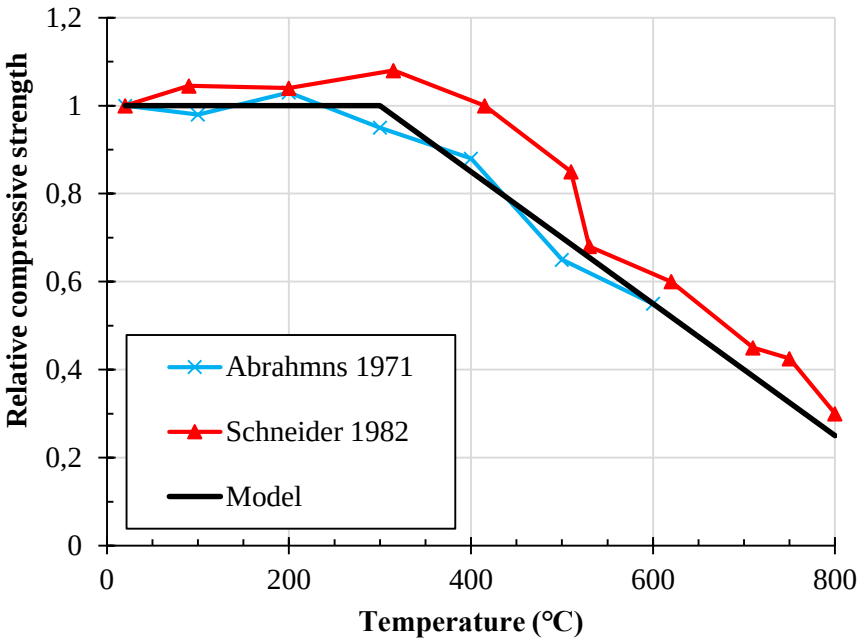

Figure 10. MASA model relative compressive strength for concrete.

This thermal degradation of compressive strength is defined as:

$$\theta = \frac{(T - T_0)}{100} \tag{2.7}$$

$$f_c(T) = \max\left(\omega_{t,f_c}\right) f_{c,0} \tag{2.8}$$

$$for \quad 0 \leq \theta \leq 2.80 \qquad \omega_{t,f_c} = 1.0 \tag{2.9}$$

$$for \quad \theta > 2.80 \qquad \omega_{t,f_c} = 1.43 - 1.53\,\theta \tag{2.10}$$

Being f_c the concrete strength at $T = 20°\text{C}$ and θ relative temperature term.

According to Bazant and Kaplan (1996) a wider range of variation occur for non-conventional aggregates this being the most important factor when it comes to evaluate the degradation of the concrete compressive strength. The fine-grained aggregates show the better behavior with temperature and calcareous and lightweight concrete show the less reduction on the strength.

2.2.3 Tensile strength

The tensile strength decrease as the temperature increases, is also an object of interest when it comes to study the concrete behavior at high temperatures. Bazant and Kaplan (1996) studied the effect of the temperature on the concrete and reported a high reduction, greater than the reduction of the compressive strength. They also indicated the high influence of the aggregate on this reduction.

According to Odelson et al. (2007) this reduction is greater because of the mismatch of the aggregate and the matrix. This effect of the aggregate type is evident from the studies of Santos et al. (2015), where it can be appreciated that the residual tensile strength for different aggregate types depends very much on the aggregate types. This difference is more pronounced for high temperatures where the strength, as observed in the Figure 11. can be three times higher for granite concrete than for calcareous concrete at 500 degrees Celsius. For temperatures about 700°C the calcareous showed no tensile strength while the granite concrete showed a 10% of the tensile strength at the reference temperature.

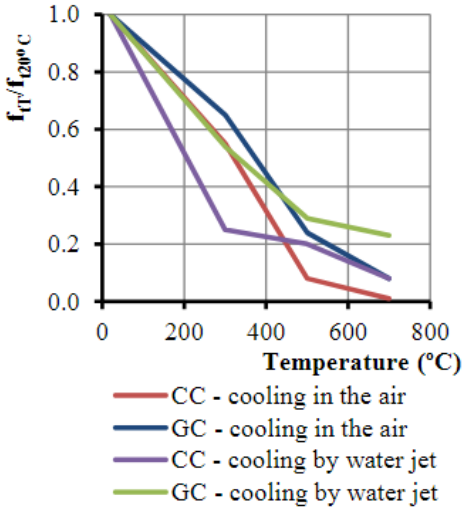

Figure 11. Concrete relative tensile strength for CC (calcareous concrete) and GC (granite concrete) for different temperatures and cooling methods

As the tensile strength is reduced significantly, in the DIN EN 1992-1-2 is recommended to assume no tensile strength for the concrete and in case of necessary, the concrete must be considered as follows:

$$f_{ck,t}(\theta) = k_{c,t}(\theta) f_{ck,t} \tag{2.11}$$

$$k_{c,t}(\theta) = 1.0 \qquad for\ 20°C \leq \theta \leq 100°C \tag{2.12}$$

$$k_{c,t}(\theta) = 1.0 - 1.0(\theta - 100)/500 \qquad for\ 100°C \leq \theta \leq 600°C \tag{2.13}$$

The decrease on the strength can be graphically observed in the Figure 12. In the numerical model, a tensile strength reduction less conservative and closer to the researches is used. This behavior for the model is defined in Periskic (2009) by:

$$f_t(T) = \max\left(\omega_{t,f_t}\right) f_{t,0} \qquad \omega_{t,f_t} = 1 - 0.13\,\theta \tag{2.14}$$

As described by Periskic (2009) this reduction in the concrete is due to the microcracks appearing on the concrete that reduce the tensile strength of the concrete to zero, in contrast to the compressive strength where the cracks do not have as much influence on the strength, since the cracks are partially closed due to the loading.

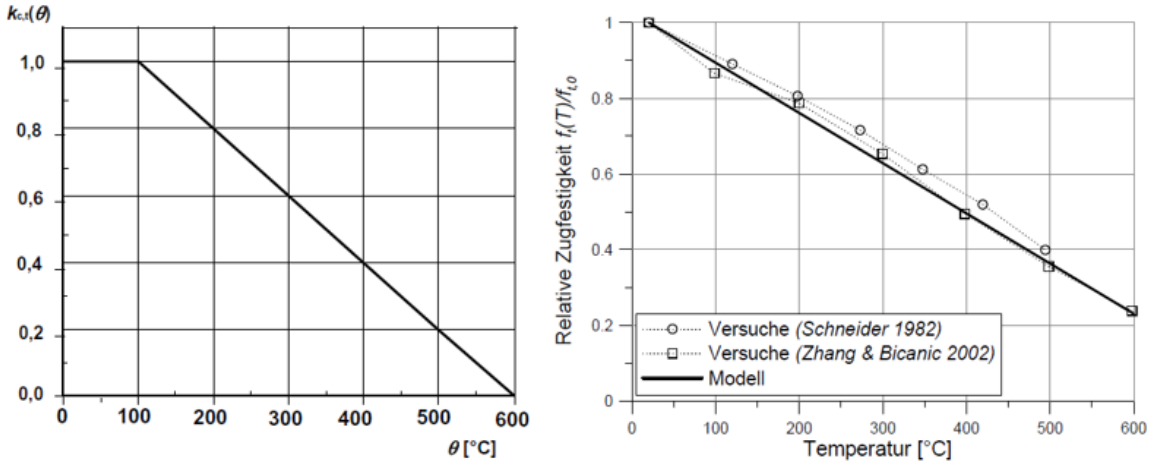

Figure 12. Concrete relative tensile strength reduction. (Left) DIN EN 1992-1-2 recommended values, (Right) MASA model.

2.2.4 Young's modulus

The Young's modulus is also influenced by the temperature changes, decreasing as the temperature increase. As reported by Odelson et al. (2007) this decrease in the Young's modulus is mainly because of the degradation of the cement paste more than the aggregates themselves. This loss in the cement paste's Young's modulus is because of both mechanical and chemical degradation of the concrete.

The model used in the numerical model follows the model proposed by Stabler (2000) reducing the concrete Young's modulus according to the following equations:

$$E(T) = \left(1 - \max\left(\omega_{t,E}\right)\right)E_0 \tag{2.15}$$

$$for \quad 0 \leq \theta \leq 10 \qquad \omega_{t,E} = 0.2\,\theta - 0.01\,\theta^2 \tag{2.16}$$

$$for \quad \theta > 10 \qquad \omega_{t,E} = 1 \tag{2.17}$$

With the previously defined value of θ, see equation (2.1).

This reduction is graphically expressed and compared with the available data test in the Figure 13.

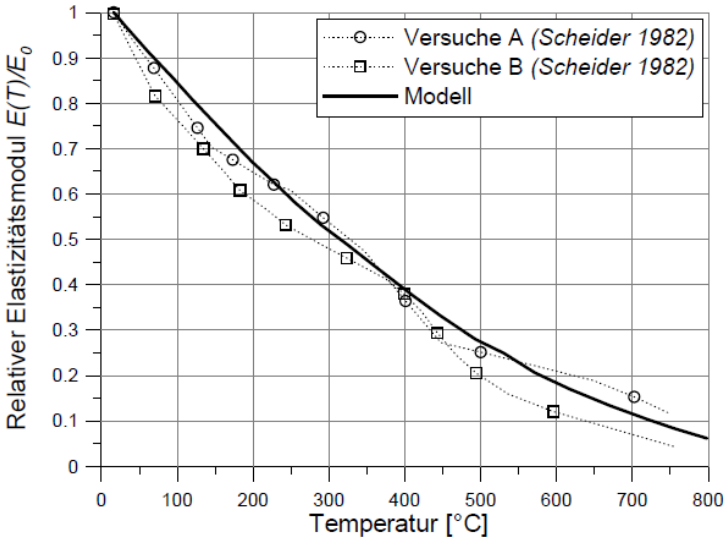

Figure 13. MASA elastic modulus reduction.

2.2.5 Heat capacity

As the concrete is a composite material and due to a temperature increase, many changes in the composition occur leading to a variation of the heat capacity of the concrete. Since there is also the water involved, and more specifically a change on the state of water, there are big variations in some transition temperatures. Apart from that, the water is also evaporated from the concrete through the cracks that increase the permeability letting the water leave the concrete changing the composition.

The concrete specific heat according to the DIN EN 1992-1-2 is the one shown in the Figure 14.

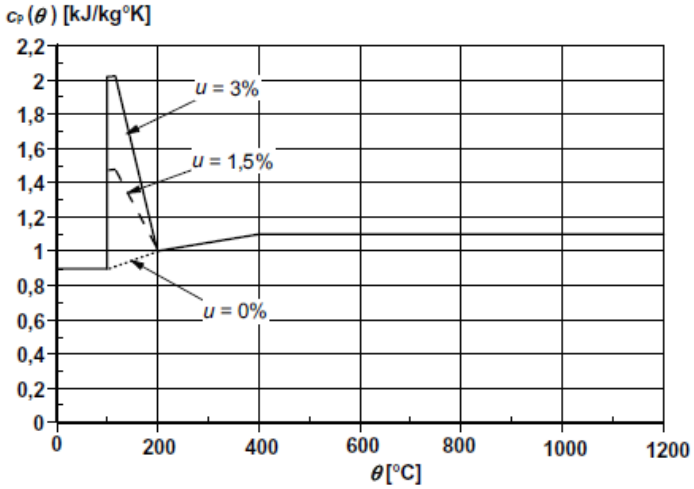

Figure 14. Specific heat of the concrete at different moisture contents.

The concrete shows a different heat capacity depending on the moisture content, which influencing at 100 degrees Celsius, temperature for which the water boils. It can also be observed that the extra energy depending on the moisture content that needs to be provided to the concrete from 100 °C to 200 °C matches with the water latent heat of vaporization. It is indicated in the code that this increased value of the heat capacity can be extrapolated for any other moisture content.

For the modelling, the values for a 0% moisture content is used for all the models.

2.2.6 Thermal conductivity

Milon et al. (2012) reported that the thermal conductivity increases as the thermal diffusivity increases, showing higher values for coarse aggregates. The thermal conductivity of the cement paste for low temperatures depends on the water/cement ratio, the degree of hydration and the moisture content.

The DIN EN 1992-1-2 also indicated that the values chosen for the high strength concrete could be higher than the ones for standard concrete as shown in the Figure 15. The thermal conductivity and the heat capacity will determine how the temperature profile will be. For higher thermal conductivity, the temperature gradient will be lower, decreasing the thermal stresses as a consequence and the concrete damage after the thermal cycle of heating and cooling.

In the case of the numerical model, the upper limit proposed by the Eurocode has been used.

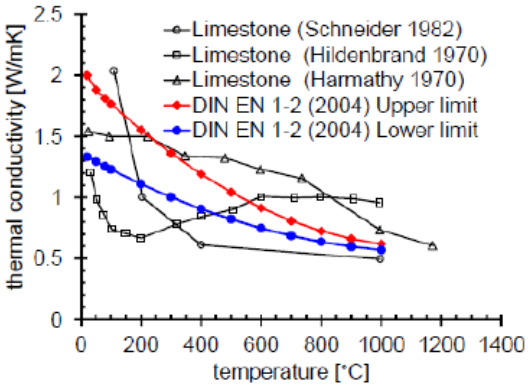

Figure 15. Thermal conductivity for the concrete, upper and lower limit of the Eurocode and experimental results.

2.2.7 Thermal expansion

The thermal expansion of the concrete or the density change must be very well defined since it determines how high are going to be the tensile stresses on the concrete due to the temperature gradient generating cracks and damaging the concrete. The aggregate has also influence in the concrete expansion this being greater for the siliceous aggregates than for the calcareous aggregates, which is highly influential since the aggregates are a

high volumetric part of the concrete and the mismatch of the matrix and the aggregates mentioned before could be aggravated. It is important to mention that as the water content of the concrete decreases as it evaporates and leaves the concrete, it influences the expansion as a consequence of the mass amount decrease. Because of this reason the thermal expansion of the concrete is compensated and not ruled only by the aggregates and matrix but also the water loss.

The thermal expansion property can also vary depending on the conditions it is measured so it introduces two new concepts which are the free thermal strain (FTS) and the load induced thermal strain (LITS).

2.2.7.1 Free thermal strain

The free thermal strain is the strain that is only a consequence of the temperature change. Schneider (1982) demonstrated that the free thermal strain largely depend on the aggregate type, being even three times greater from quartzite to expanded clay as shown in the Figure 16 b). Since the aggregates are by far the most abundant material in the concrete (65-70%), a high dependence of the thermal strain on the aggregate should be expected.

Depending on the concrete, there could be a high mismatch of dilatations depending on the cement paste used. Cruz and Gillen (1980) studied the cement paste thermal strain for high temperatures and compared with the different mortars. These results are shown in Figure 16 b) seeing that the thermal strain of the cement paste varies very much from the one of the mortars. When compared the thermal strain of the concrete with the thermal strain of the aggregates an incompatibility is observed which in the reality influences the mechanical damage that has been mentioned before.

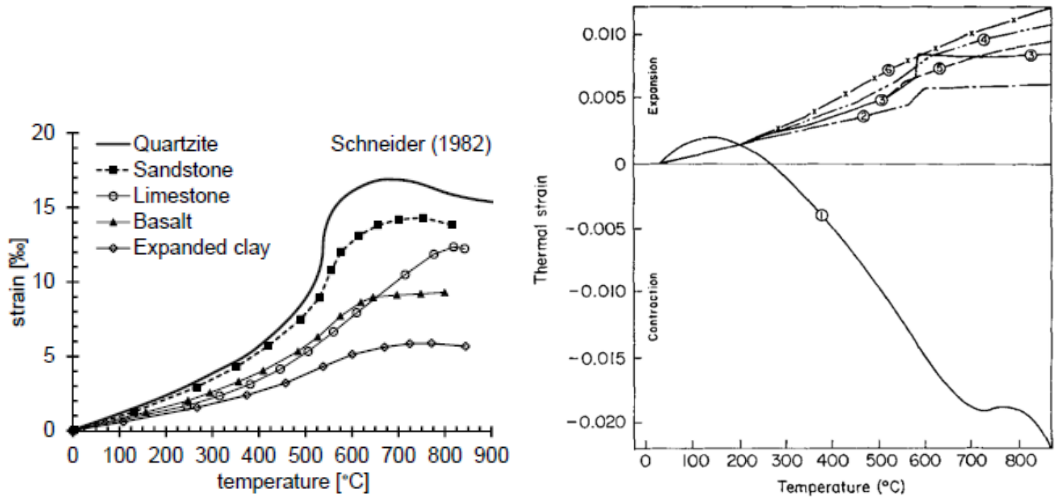

Figure 16. (Left) Thermal expansion for different aggregates. (Right) Thermal expansion for different cement pastes, concretes and aggregates 1) Portland cement paste, 2) Elgin sand mortar, 3) Ottawa sand mortar, 4) Elgin sand and gravel concrete, 5) Elgin sand and crushed dolomite concrete and 6) dolomite rock.

Another important property of the concrete when measuring the after-fire stresses is the thermal cycle residual strain. This property was studied by Sullivan et al. (1986) for different aggregates demonstrating (Figure 17) that after heating a residual thermal strain can remain and therefore, thermal stresses. It can also be observed that for relatively low heating the residual thermal strain is lower than it is for higher temperatures.

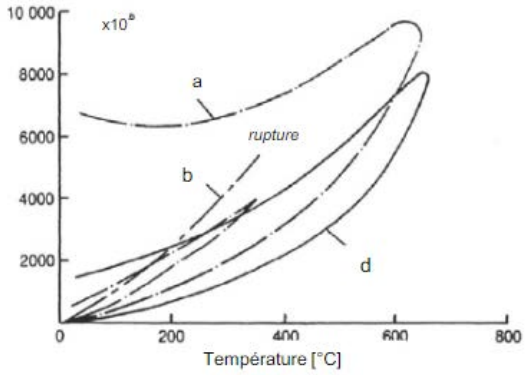

Figure 17. Thermal strain after a heating-cooling cycle for different aggregates a) calcareous b) quartz c) siliceous

Hager (2004) also performed different studies for the heating rate of 0.5°C/min and 1°C/min for both siliceous and calcareous aggregates obtaining the results shown in the Figure 18.

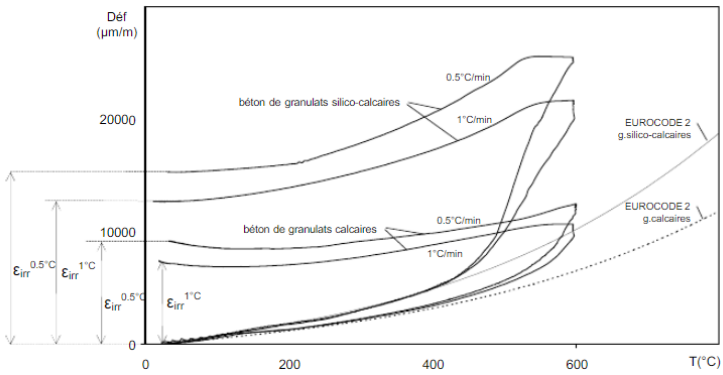

Figure 18. Residual thermal strain for concrete made of different aggregates.

The free thermal strain has been manually set according to the values plotted in the Figure 19. The residual thermal strain after a thermal cycle is considered to be zero. This property should not have a big influence in the mechanical damage evaluation but in case to be considered, it would influence in the damage making the thermal gradients be more influential because of the difference in strains at different temperatures. The effect of the residual expansion is not considered in the Eurocode.

There are also some other approaches like curve defined by Periskic (2009) according Bazant and Kaplan (1996) being determined by the following equations:

$$\dot{\varepsilon}_{ij}^{ft} = \alpha\, \dot{T}\, \delta_{ij} \tag{2.18}$$

$$for \quad 0 \le \theta \le 6 \qquad \alpha = \frac{6.0\ 10^{-5}}{7.0 - \theta} \tag{2.19}$$

$$for \quad \theta > 6 \qquad \alpha = 0 \tag{2.20}$$

The curve used in the model is plotted in the Figure 19 with different experiments results from Schneider (1982).

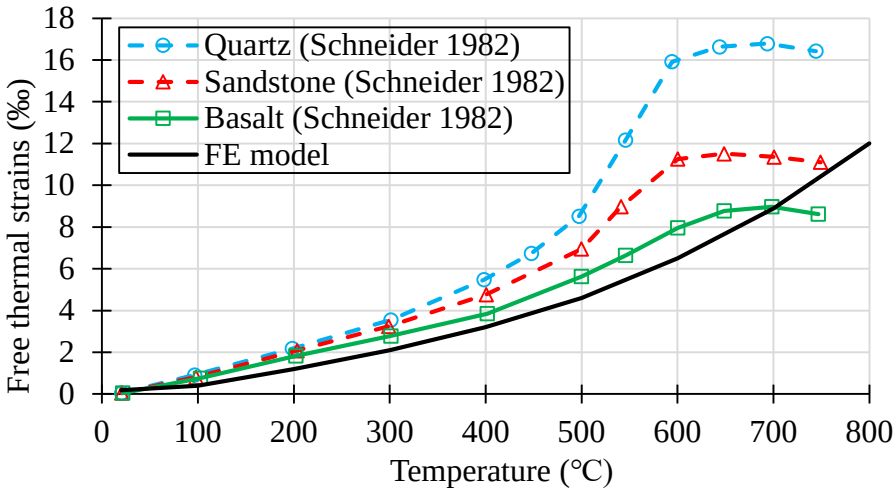

Figure 19. Model free thermal strain and different models performed for different aggregates.

2.2.7.2 Load induced thermal strain

Load Induced Thermal Strain also referred to as Transient Thermal Creep is an effect occurring in the concrete while heated under load. This effect induces an extra strain due to the load applied while heated, which is bigger as the load is increased. Anderberg & Forsen (1982) studied the effect of the load factor and its influence over the LITS can be seen in the Figure 20. It can be observed that the effect is much bigger as long the load factor is increased. Even if it is not plotted in the, for a load greater than a 40% we have a big reduction for high temperatures, which is clearly not linearly proportional to the load factor.

The results showed in the Figure 20 also show the free thermal strain of the concrete which means that the strain for a service load of a 45% at 500°C the strain would be about a 1% and for 100°C more can be about a 2%. This study is critical since some elements that can be exposed during fire like columns can reach these temperatures and therefore, these high strains.

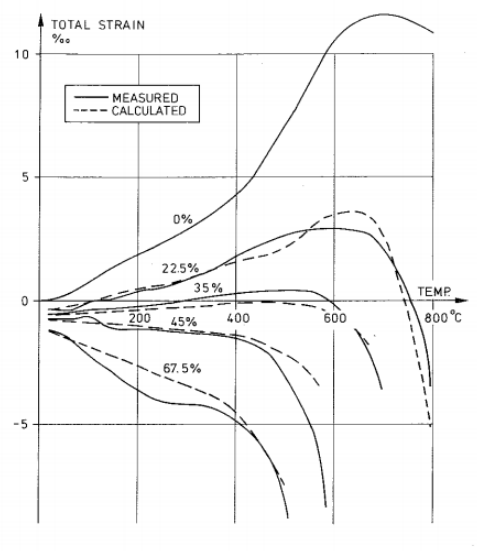

Figure 20. Thermal strain for unloaded and loaded concrete specimen.

This load induced thermal strain can be extracted from the graphs considering the free thermal stress, which is also defined as transient thermal strain and can be observed in the Figure 21 obtained from Hager (2004) data.

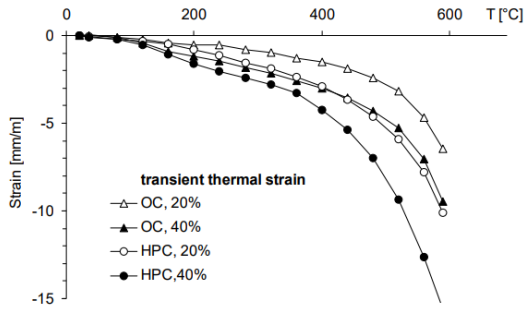

Figure 21. Transient thermal strain for ordinary concrete and high-performance concrete.

It was also studied by Mindeguia et al. (2013) this effect for tensile loads but no load induced strain was observed limiting this effect to the compressive stresses. It was also reported that for temperatures up to 400°C the LITS is originated from the drying and dehydration of the heated concrete and for temperatures higher than 400°C it is mainly driven by the micro cracking caused from the materials incompatibly mentioned before.

2.2.8 Fracture energy

The fracture energy is a property that does not vary as much as the others. It was studied for temperatures up to 600°C by Zhang and Bicanic (2002) reporting that there is an increase for temperatures up to 300°C and then decreased again for temperatures up to 600°C. They reported that the evaporation of the capillary water had a high impact on this

property variation, but it was mostly affected by the evaporation of the gel water and chemically bound water making the fracture energy decrease.

In the model the relative fracture energy is defined by the following equations, being $G_F(T)$ the fracture energy for a specific temperature:

$$G_F(T) = \max\left(\omega_{t,G_F}\right) G_{F,0} \tag{2.21}$$

$$for \quad 0 \leq \theta \leq 2.8 \qquad \omega_{t,G_F} = 0.917 + 0.467\,\theta - 0.0833\,\theta^2 \tag{2.22}$$

$$for \quad \theta > 2.8 \qquad \omega_{t,G_F} = 1 + 0.407\,\theta - 0.0727\,\theta^2 \tag{2.23}$$

The model tries to fit the results obtained by Zhang and Bicanic (2002) as it is shown in the Figure 22.

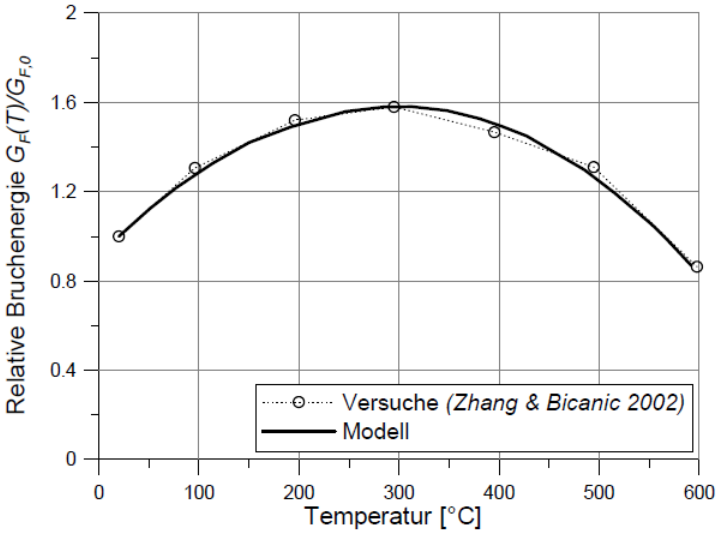

Figure 22. MASA values for relative fracture energy for concrete.

2.3 Steel properties depending on the temperature

The variation of the steel properties considered in the FE model can be observed in the Figure 26 and Figure 27. The element type used for the steel elements the steel is not going to cause the failure and the steel behavior is not the object of this study, it will not be detailed the causes for this degradation.

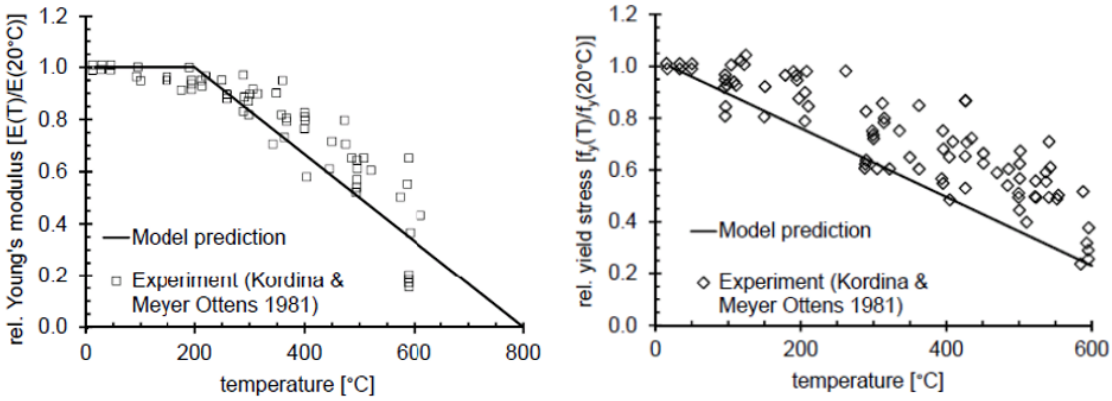

Figure 23. (Left) steel Young's modulus reduction (Right) steel yield stress reduction.

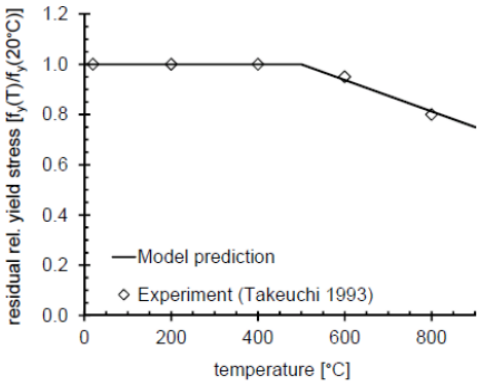

Figure 24. Residual yield stress for steel.

2.4 Effect of the high temperatures on the steel and concrete interaction

The properties of the structural steel also depend on the concrete properties. The behavior of the steel depending on the temperature and the different microstructure changes have been very accurately defined. As expected, there is also as reduction in the mechanical properties of the concrete for high temperatures which will be more detailed later.

As mentioned before, the expansion incompatibilities between the cement paste and the aggregates can create thermal stresses leading to cracks, damaging the concrete and reducing the strength and its mechanical properties. For the steel-concrete this incompatibility is also an issue but only for very high temperatures (more than 550-600 degrees Celsius), the deformation of the steel is very close to the one of the concrete (the siliceous aggregate concrete), minimizing the negative effects it could create. The thermal expansion values recommended by the Eurocode for different temperatures are plotted in the Figure 25. For the Calcareous aggregate the deformation is not matching that well for temperatures below 550-600 degrees Celsius, as the siliceous aggregate did, and the mismatch of the strains could create high stresses even for not very high temperatures.

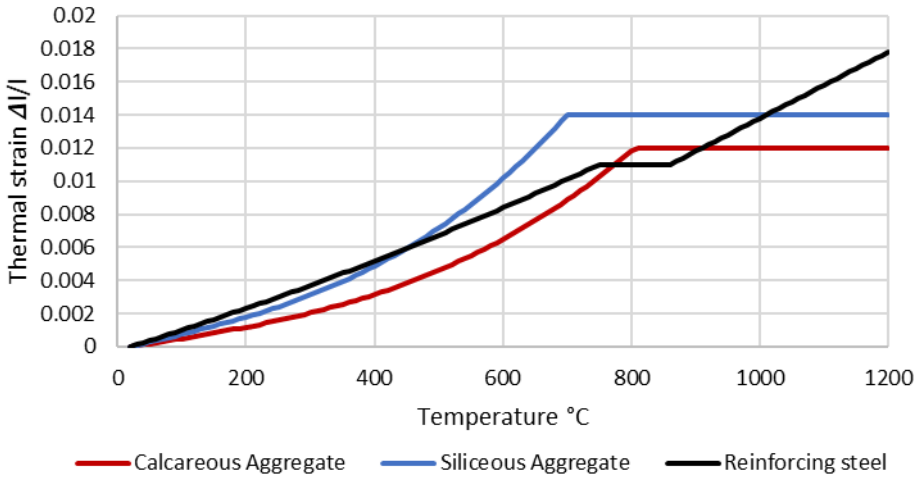

Figure 25. Steel and different aggregates concretes thermal expansion for different temperatures.

As we increase the temperature a reduction in the steel properties must be considered. According to Bošnjak (2014) this reduction in the mechanical properties is also considered in the MASA software as plotted in the Figure 26. The results are validated by the experiments performed by Kordina and Meyer-Ottens (1981). In the Figure 27 the residual yields stress is also shown. Should be mentioned that the residual yield stress will depend very much on the cooling rate since while cooling a thermal process is being applied to the concrete altering the properties and microstructure.

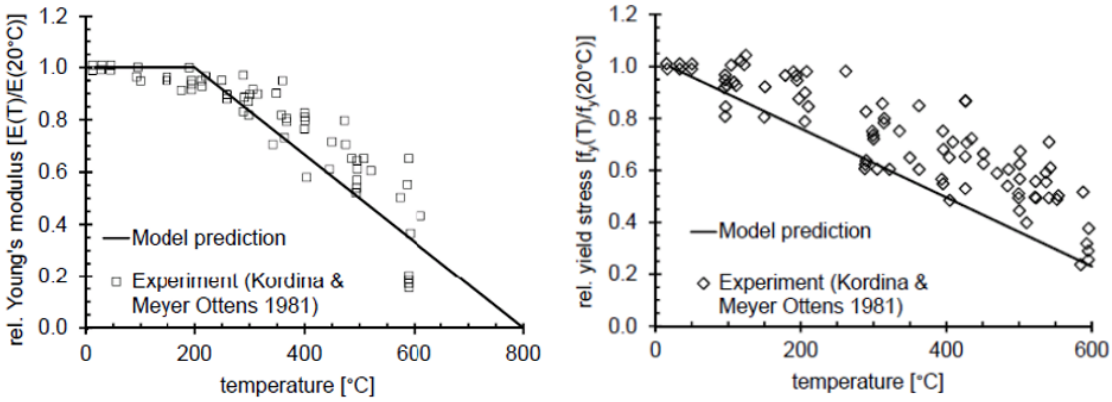

Figure 26. (Left) steel Young's modulus reduction (Right) steel yield stress reduction.

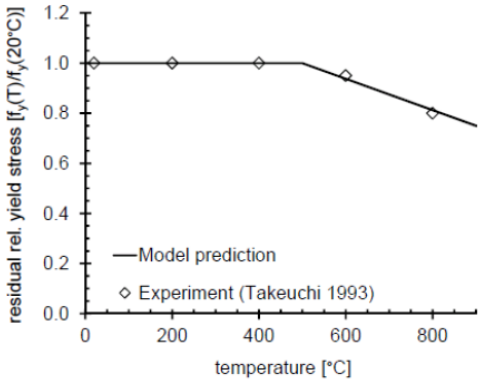

Figure 27. Residual yield stress for steel.

2.5 Microplane model

2.5.1 General Aspects

The microplane model in comparison to the more popular finite element method, is based in the decomposition of the element in numerous planes that are working in a microscopic level (see Figure 28). The definition of the stress and strain components will define the behavior at macroscopic level. These planes can be understood as the planes existing between the aggregates. This method shows are more effective performance than the finite element method because the classic local smeared fracture analysis, is mesh dependent (Bazant and Prat (1988). The bigger the mesh size, the bigger the energy consumption, so for big elements, the crack will not be realistically reproduced, for this reason, a model with no dependence on the mesh size is needed. Because of this, a so-called localization limiter is introduced. According to Ozbolt et al. between the different approaches that are in use, the smeared crack approach is the more general approach, especially for engineering applications.

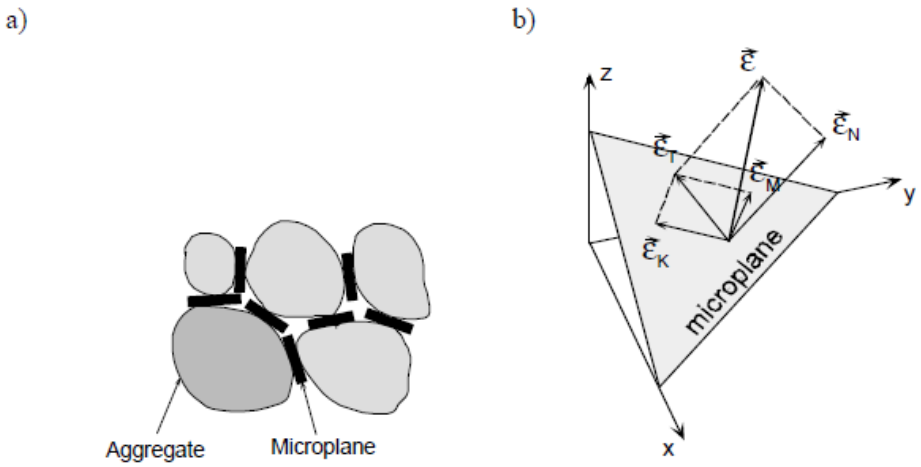

Figure 28. Microplane model and microplane components.

In the microplane model, the normal stresses are decomposed in the volumetric and the deviatoric part. According to Ozbolt, for a good performance this deviatoric compressive strength and the shear strength need to be set 10 times larger than the volumetric and deviatoric tensile strength. The problem is that this model shows a pathological problem when the crack happens. According to Jirasek (1993) the main problem is related to the split of the normal microplane component into volumetric deviatoric part. For a better understanding of the problem how these planes are working is shown in the Figure 29.

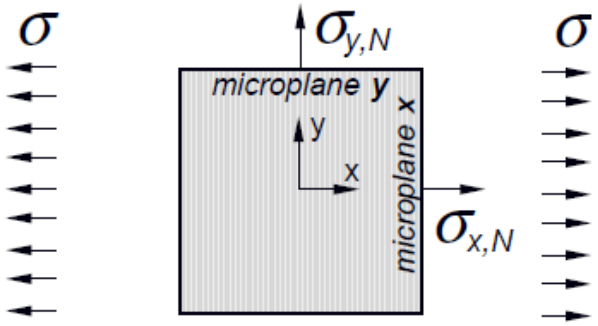

Figure 29. Microplane model components loaded in uniaxial tension.

If we only consider the **x** and **y** planes where **x** is oriented in the load direction and the **y** is perpendicular to it. As said before, this normal microplane component in the plane **y** is divided in the volumetric $(\sigma_{N,y}, \varepsilon_{N,y})$ and deviatoric $(\sigma_{D,y}, \varepsilon_{D,y})$ stresses and strains shown in the Figure 29. Therefore, the total stresses and strains will be defined as:

$$\varepsilon_{N,y} = \varepsilon_V + \varepsilon_{D,y} \tag{2.24}$$

$$\sigma_{N,y} = \sigma_V + \sigma_{D,y} \tag{2.25}$$

And the relationships between the volumetric strains and the deviatoric strains are defined as:

$$\varepsilon_V = 1/3(1 - 2v)\varepsilon_x \tag{2.26}$$

$$\varepsilon_{D,y} = -1/3(1 + v)\varepsilon_x \tag{2.27}$$

And the secant stiffness moduli:

$$\sigma_V = C_V \varepsilon_V \tag{2.28}$$

$$\sigma_{D,y} = C_D \varepsilon_{D,y} \tag{2.29}$$

But as said before this model present a pathological problem, this happens when the crack occurs and the deviatoric stress and strain components of plane **y** reduce to zero as well as the σ_V. Considering the behavior of the microplane defined by the stress-strain curves of the Figure 30. As we have defined, the relationship between the deviatoric strain and the axial strain is defined by the equations (2.26) and (2.27) With the compressive strength considered 10 times larger than the tensile, the only possible way to fulfill the equations is when the $\varepsilon_{D,y} = 0$, which would predict a lateral expansion of the model.

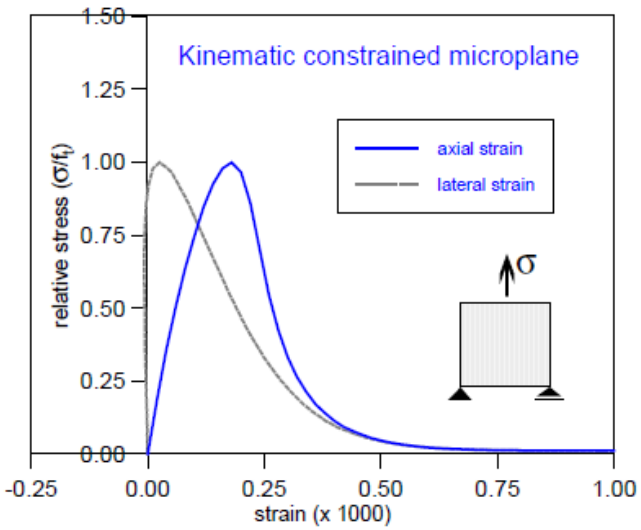

Figure 30. Bazant and Prat's kinematic constrained microplane stress strain curve.

Defining $\eta = (1 - 2v)/(1 + v)$, the following relationship can be determined:

$$C_{D,y} = \eta C_V \tag{2.30}$$

This expression indicates that for the previous equations to be fulfilled the relationship between the deviatoric component and the volumetric needs to be constant. To give to the model a more realistic behavior, the discontinuity of the strain field must be considered. The relaxed kinematic constrains try to avoid this pathological behavior to happen. According to Ozbolt et al. (2001), there are two different ways to do this, one is to impose the static constrain approach at the microplane level or keep the kinematic constrain approach but modifying the microplane strain components by adopting additional constrains.

Bazant et al. (1996) proposed a microplane model with "stress-strain boundaries" in which the microplane components have a stress limits and depend on the macroscopic stress tensor. Some other methods have been also proposed with a good performance and realistically good behavior but according to Ozbolt et al. (2001) the simplicity is lost.

2.5.2 Relaxed kinematic constrains

According to Ozbolt et al. (2001) with this approach the simplicity is kept by using most of the assumptions of Bazant and Prat (1988) and Ozbolt and Bazant (1992), which are the following:

I. As mentioned before, each plane resists the normal and shear strains components. For the case of the normal they are decomposed in the volumetric

and deviatoric parts and the shear is divided in another two perpendicular components.

II. Except the volumetric strain, the microplane strains are resolved by the macroscopic strain tensor ε_{ij} multiplied by the function ψ.

III. The value of ψ reflects the discontinuity due to the discrete tensile cracking, it ensures a good transition with realistic values from dominant tensile strain to dominant compressive load, it is assumed to depend on the principal tension stress. The value of ψ varies from 0 to 1, it is applied for each microplane and the value is chosen depending on the volumetric stress strain relationship.

IV. The shear response on each microplane is assumed to be dependent on the volumetric strain for the correct modelling of concrete at high pressures.

To generate a good macroscopic response (stiffness and stress) the microplane stress and stresses need to be integrated (Ozbolt and Bazant, 1992). The equation of equilibrium by the virtual work equation is defined as:

$$\frac{2\pi}{3}\sigma_{ij}\delta\varepsilon_{ij} = \int (\sigma_N \delta\varepsilon_N + \sigma_M \delta\varepsilon_M + \sigma_K \delta\varepsilon_K)\Omega(\boldsymbol{n})\, dS \tag{2.31}$$

Where **n** is the unitary normal vector to the microplane. The left-hand side term indicates the macroscopic work and the $\Omega(\boldsymbol{n})$ is the weight function that introduces the anisotropy of the material in the initial state. For normal concrete $\Omega(\boldsymbol{n})$ is assumed to be 1, which implies isotropy, but for other materials the anisotropy could be set by using this weight function such as the one shown in Figure 31. Generally, two different types of anisotropy exist, one which is the initial anisotropy and the damage induced anisotropy. The second one is due to the localization of the damage in a particular direction caused by a loading. This is also considered in the stress-strain dependent constitutive laws.

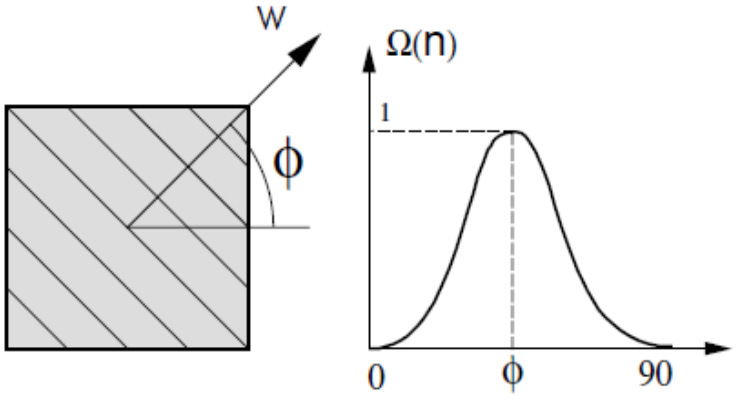

Figure 31. Initial anisotropy as a function of the angle ϕ.

Some improvements have been proposed by Carol and Bazant (1997) introducing new terms and variations for a better behavior of the model. For more details, check Ozbolt et al. (2001).

As specified in Ozbolt et al. (2001) the model has 15 parameters that have been calibrated experimentally, even if they have a physical meaning, they have no any relationship with the macroscopic behavior of the concrete. Only four parameters need to be set to define the concrete behavior which are automatically generated by the macroscopic properties set by the user which define the microplane properties and make it functional.

2.5.3 Thermal strains of the microplane model

For the calculation of the total strain, the different strains created by the thermal analsys must be considered. This strains are mainly three, the ε_{FTS} which is the strain that is created because of the free thermal strains, the ε_{LITS} which is the load induced thermal strain and the ε_{creep} which is the thermal strain created by the creep effect. The sum of all this strains will determine the thermal strain created by the heating.

$$\varepsilon_{total} = \varepsilon_{FTS} + \varepsilon_{LITS} + \varepsilon_{creep} \tag{2.32}$$

When a load is applied, a new strain is introduced which is the mechanical strain. This strain can be divided into the elastic, plastic and damage strain. In this model, the strains are obtained from the constitutive law. The free thermal strains that are used in this model are defined in the Figure 19.

3 Study

The main objective of this thesis is the numerical investigation of bond behavior after exposure to elevated temperatures. In order to validate the numerical model, the numerical analysis was first performed for a series of tests performed by Bosnjak et al. 2017). A short overview of the experimental study used for the validation is presented in the next section.

After the validation, an extensive numerical study was performed in order to investigate the effect of concrete cover, strength, bond length on the bond performance after exposure to elevated temperatures. The modelling approach and the obtained results are presented in Section 3.1.

3.1 Previous experimental studies

For the analysis of the bond strength reduction after slow heating Bosnjak et al. (2017) casted different cuboidal test specimens being square prisms sized in 160 mm x 160 mm x 300 mm. The bond length was set to 8 times the diameter, as an uniform bond stress was assumed to be achieved through the whole bond and avoid the localization of the stresses as it would happened for long bond lengths (This variation on the bond performance depending on the bond length is also studied in the numerical analysis). In Figure 32 the five different rebar layouts are shown corresponding to the specimens tested.

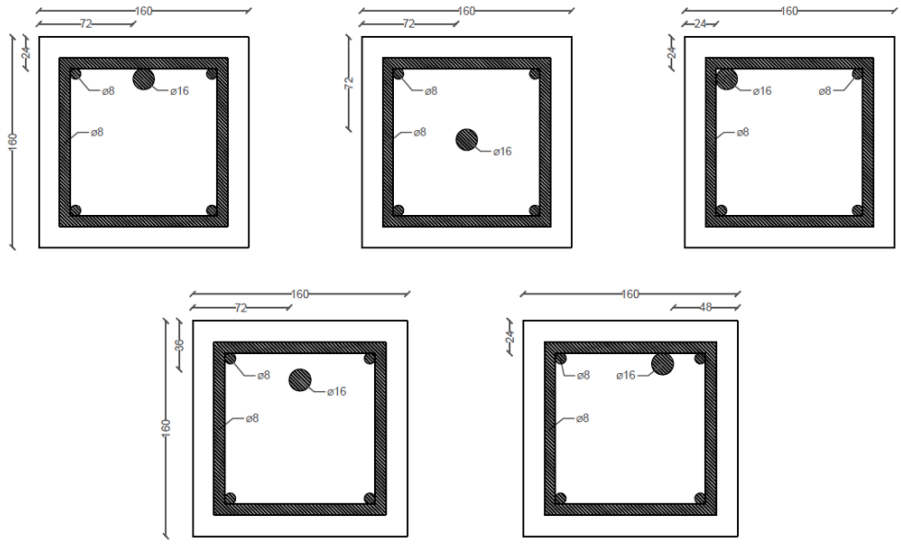

Figure 32. Rebar position in the tested specimens.

The first one was a centered rebar with a cover of 72 mm from all sides where the pure bond failure was expected to happen so a maximum strength for the pure bond failure could be obtained. There were also tested another four rebar positions with the following c_{min}/c_{max} so the total rebar positions tested are showed in the Table 1.

c_{max}	c_{min}	c_{min}/c_{max}
72 mm	72 mm	1
72 mm	36 mm	1/2
72 mm	24 mm	1/3
48 mm	24 mm	1/2
24 mm	24 mm	1

Table 1. Different rebar positions tested.

The specimens have also transversal and longitudinal reinforcement to achieve a certain level of confinement. The Figure 33 shows the distribution of the reinforcement in the specimen. The specimen had a debonded length of 7ds, a bonded zone of 8ds in the center and finally 60 mm of debonded length.

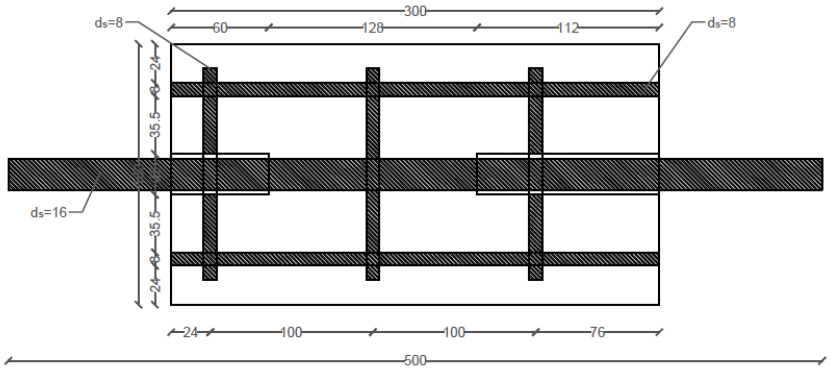

Figure 33. Cross section of the test specimen.

These specimens were heated to the temperatures of 300°C, 500°C and 700°C and tested after cooling. The heating rate was of 2°C/min until the maximum temperature was reached, then it was remained at the maximum temperature for 2 hours to achieve a uniform maximum temperature in the whole specimen and cooled down to the ambient temperature with a cooling ratio of 2°C/min.

The concrete used was a C16/20 concrete tested with standard 150mm cubes at the age of 28 days showing a strength of 23MPa. All the specimens were tested at the age between 28 and 35 days. The results obtained by the tests are the ones showed in the Figure 34, Figure 35 and Figure 36.

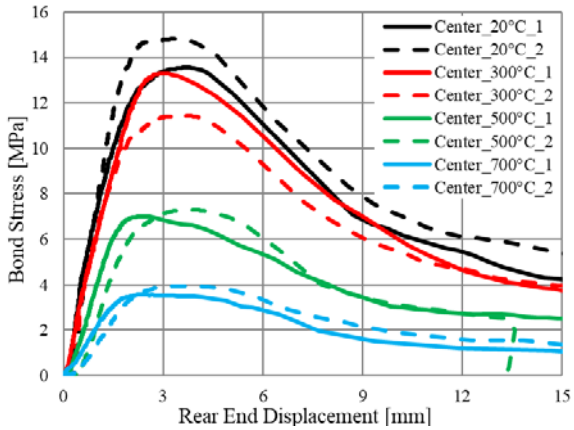

Figure 34. Bond stress-slip curve for pull-out center tests after heating to various temperatures.

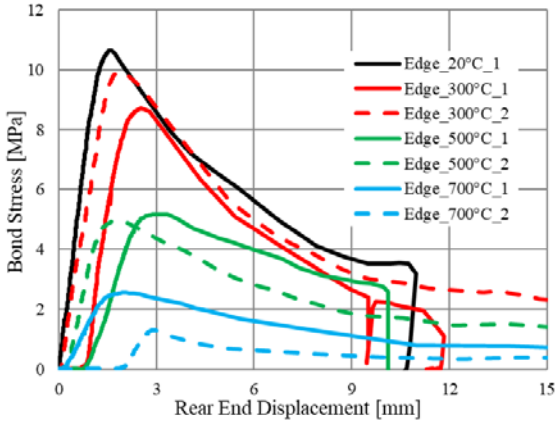

Figure 35. Bond stress-slip curve for pull-out edge tests after heating to various temperatures.

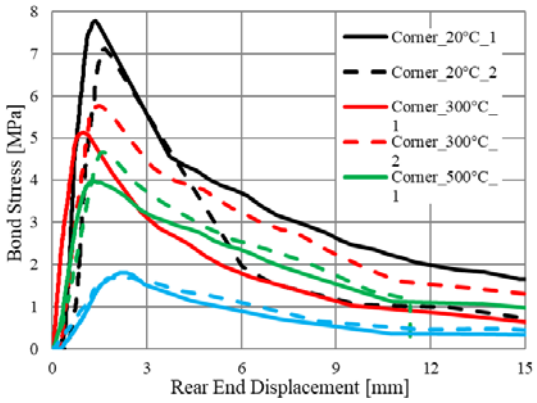

Figure 36.Bond stress-slip curve for pull-out corner tests after heating to various temperatures.

It can be observed that as the cover is reduced the bond strength is reduced critically, being about the 50% for the reference temperature if the center-positioned rebar is compared with the edge positioned rebar. The cracks observed after the tests showed that

for all the specimens but the one in the center positioned rebar, the splitting was the failure mechanism.

For the center positioned rebar it was observed that at 300°C the reduction was relatively low, being a greater difference when the temperature reached 500°C reducing by a 50% the peak load. At temperatures of 700°C only about a 30% of the strength at the reference temperature is showed. The Young's modulus is also greatly reduced by the increase of the temperature. This decrease on the Young's modulus follows also the same reduction tendency showed by the bond, being almost no decrease for temperatures up to 300°C. For temperatures of 500°C and 700°C there is a much greater decrease in the Young's modulus.

This reduction in the bond strength is higher for the model in the edge and the corner since the splitting is the failure mode which is governed by the tensile strength. As explained before, the reduction in the tensile strength is much greater than any other properties which makes the bond strength to decrease in more than a 50% for the edge at 500°C and to the 25% for the corner and edge at 700°C.

The degradation of the peak bond stress depending on the temperature for different rebar positions is shown in the Figure 37.

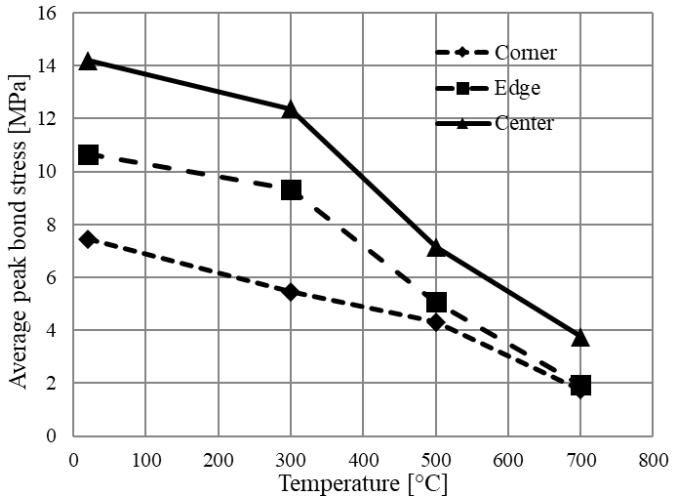

Figure 37. Degradation of the peak bond stress as function of temperature for different rebar positions.

3.2 Numerical study and Models

3.2.1 Modelling

In the numerical analysis six different models were made with the five rebar positions mentioned before and an extra one with a rebar position closer to the center to analyze the transition from pure pull-out failure to splitting. The modelled specimens with the different rebar positions are shown in the Figure 38.

Figure 38. Rebar positions for the numerical models.

The models are prisms of 160 mm x 160 mm x 300 mm. The diameter of the test rebar is 16 mm. For the confinement the specimens have reinforcement, both transversal and longitudinal being 8 mm diameter bars, in the specific case of the corner, the longitudinal reinforcement in the corner of the rebar is substituted by the rebar. The bond has two different parts as shown in the Figure 33 being a distance of eight times the diameter the bonded length (128 mm) and the rest, debonded, with a front debonded length of seven times the diameter. This debonded length was chosen to avoid local effects in concrete.

Concrete was modelled using tetrahedral elements and steel of the test rebar using Linear-elastic hexahedral elements have been used for the rebar. For the bond modelling, bar elements have been used and between the steel and the concrete, hexahedral elements have been used as a contact layer to achieve continuity for numerical reasons.

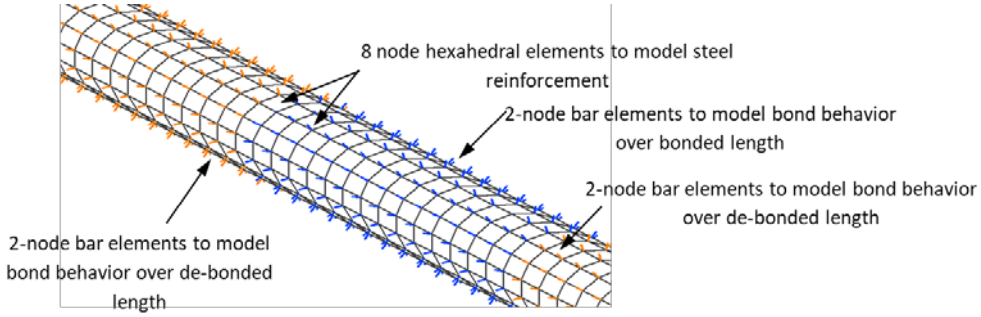

Figure 39. Bond elements.

The bar elements can be observed in the Figure 39. These elements connect the rebar elements with the concrete elements and provide the necessary strength in terms of shear force to transmit the bond strength the ribs would transmit in the real behavior. Apart from that, also debonded bar elements are used in the part that is not bonded for which only the axial force is transmitted but no shear. These bond elements are not temperature dependent, i.e. no thermal degradation of bond strength was considered.Setting the elements this way, all the bond strength reduction will be as a consequence of the concrete strength reduction because of the temperature.

Boundary conditions and the reinforcement cage can be seen in the Figure 40.

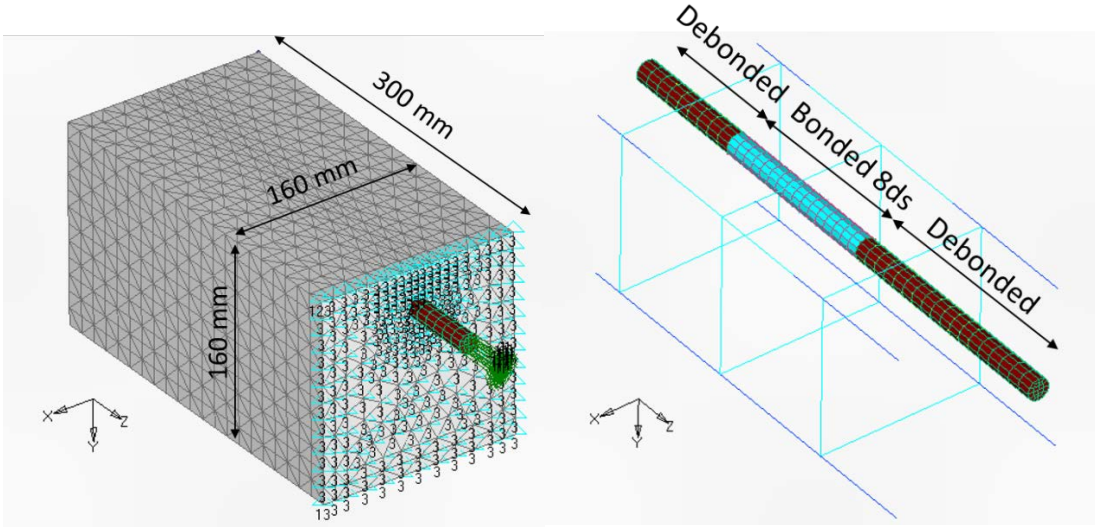

Figure 40. Model constrains and forces (left) and model rebar and reinforcement disposition (right).

A total of six different models have been modelled, with the different rebar positions indicated in the Table 2 and these six rebar positions have been calculated for five different rebar positions and for four different temperatures being the reference temperature, 20°C and for 300°C, 500°C and 700°C. At the end, a total amount of 120 models have been calculated for the parametrical analysis.

Cmax (mm)	Cmin (mm)	Cmin/Cmax
72	72	1
72	48	2/3
72	26	1/2
72	24	1/3
48	24	1/2
24	24	1

Table 2. Different rebar positions and cover ratios.

In the Figure 41 all the models can be observed and the different rebar positions.

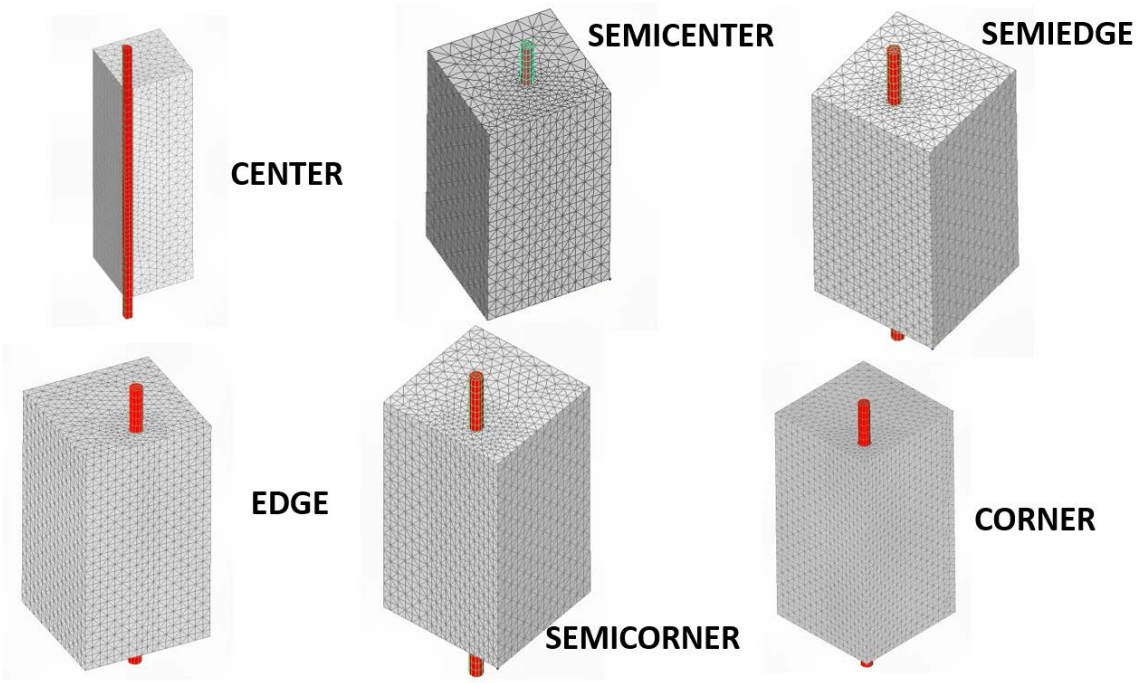

Figure 41. FE models.

3.2.2 Materials properties

3.2.2.1 Concrete

As the validation is wanted to be achieved the same properties as the concrete used in the previous experimentation have been set. For the compressive strength 20 MPa has been set. For the calculation of the tensile strength the equation (*3.4)* has been used giving a value of 2.2 MPa. For the elastic modulus of the concrete the equation (*3.2* obtaining a value of 21000 MPa. For the concrete fracture energy, the equation (*3.3* has been used obtaining a value of 0.05 N/mm. The Poisson's ratio was also set to 0.18.

$$f_t = 0.3\, f_c^{0.67} \tag{3.1}$$

$$E_c = 4700\, \sqrt{fc} \tag{3.2}$$

$$G_f = 6\, f_c^{\,0.7} \tag{3.3}$$

In the case of the concrete, as mentioned before the properties are temperature dependent and the values depending on the temperature have been previously represented.

For the concrete a mesh size about 10 mm has been used in the surrounding concrete and for the bond nearby a mesh size about 6 mm has been used.

3.2.2.2 Steel

For the steel elements a linear elastic elements have been used with an elastic modulus of 200000 MPa and a Poisson's ratio of 0.33. Since no strength has been defined, no failure will occur in the steel. The strain, conductivity, and heat capacity are also defined for the steel and how they vary for the different temperatures for which the values according to the Eurocode have been used.

3.2.2.3 Bond bar elements

For the bond elements, bar elements have been used. The behavior of this bar elements are defined in the Figure 42 with the following values: a maximum τ_{max} which is the maximum shear force it will transmit between the steel and the concrete, an s_1 which is the strain for which this value will be reached. After reaching that maximum shear stress the transmitting shear stress remains constant until a defined s_2 after which the bond stress starts decreasing until a residual value τ_R in an specific s_3 after which a constant value of the stress is transmitted for any strain. The properties for the bond elements do not vary depending on the temperature.

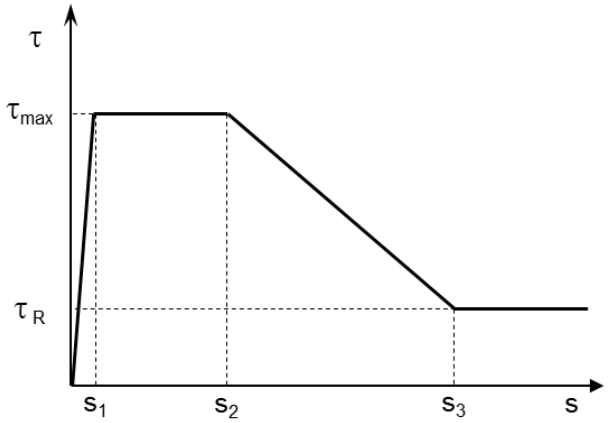

Figure 42. Bar elements stress-strain.

For this values a τ_{max} of 13.50 MPa was set and a τ_R of 5.4 MPa with a s_1, s_2 and $s_3$of 0.05, 1.5 and 6.0 respectively.

3.2.3 Validation

For the validation the models were compared with the results in the tests from Bosnjak et al. 2017) after exposure to different temperatures as well as in reference case (no thermal exposure) . For the pull-out model a displacement rate of 0.025 mm per step was applied. The results for the test rebar in the center (pure pull-out failure) are shown in the Figure 43.

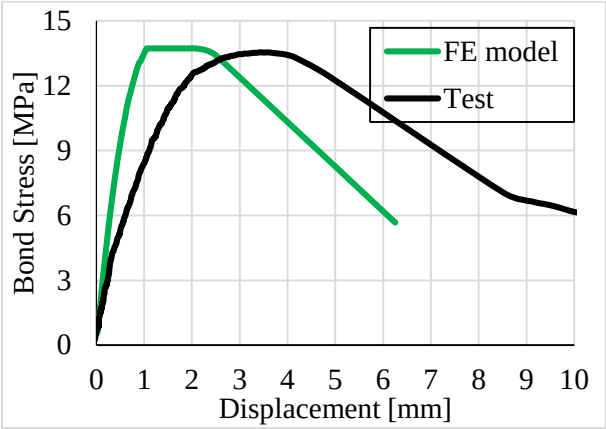

Figure 43. Rebar center located FE model vs Test

Since this is a pull-out failure and the bond elements strength has been stablished based on the test, the same strength should be expected. In the Figure 44 it can be observed how the failure mode matches and the pure pull-out failure is being the failure mode. Red color represents a crack width of 0.1 mm, which is considered as critical crack width for concrete.

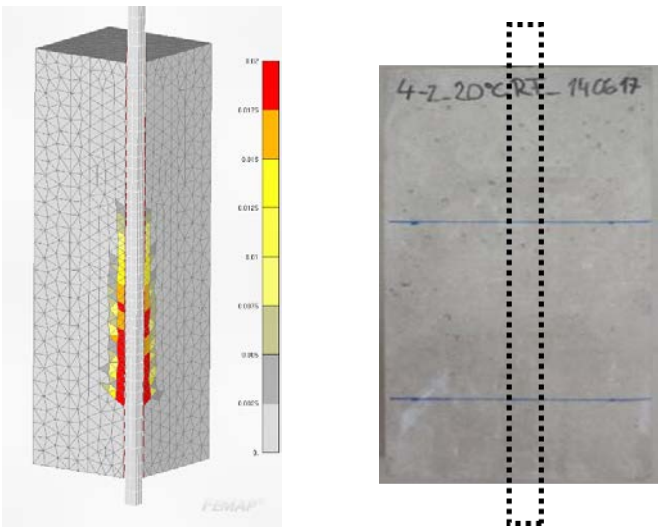

Figure 44. FE model cracks vs experiment for the center case.

The results of the finite element (FE) models vs. the experiment for the rebar at the edge and corner, respectively, can be observed in the Figure 45.

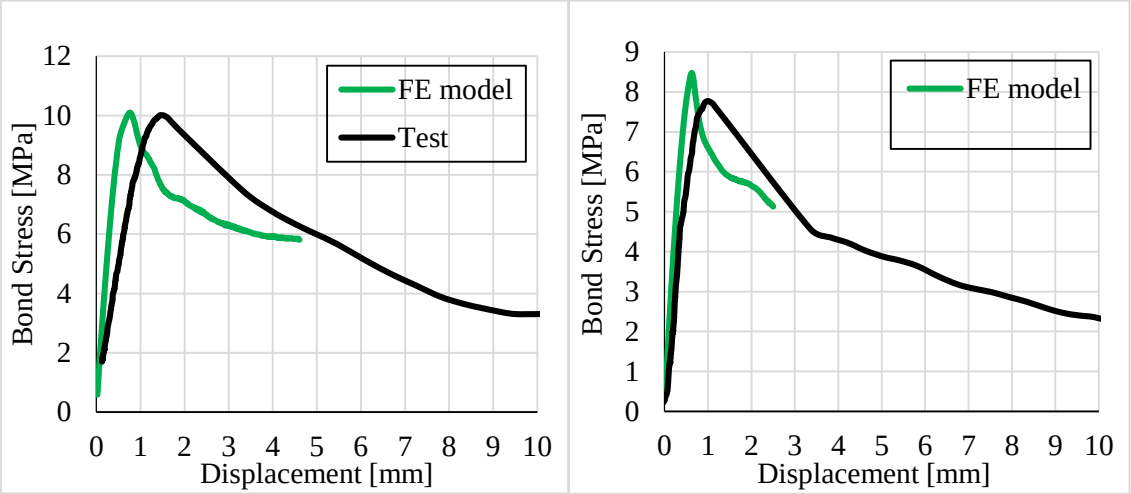

Figure 45. FE model vs Test for edge (left) and corner (right)

It can be observed that the strength values are reduced since in this case the splitting is happening and the full bond strength will not be reached. For the case of the edge a higher value has been obtained and a lower value than for the corner model, as it was expected because the as seen before the splitting strength depends on the relationship between the maximum and the minimum cover. For the failure mode of the edge it can be observed in Figure 46 how it matches and a crack is developed in the outer face close to the rebar. It can be concluded that the numerical model is able to realistically reproduce the experimental data.

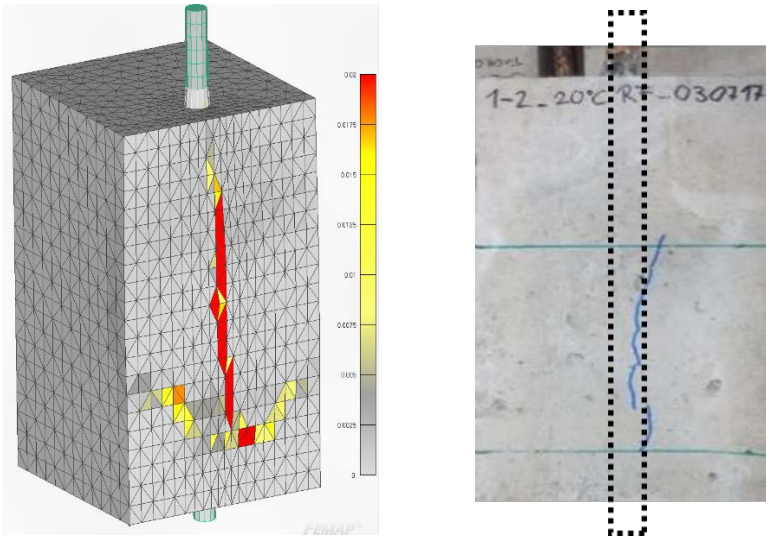

Figure 46. FE model crack vs experiment for the edge located rebar.

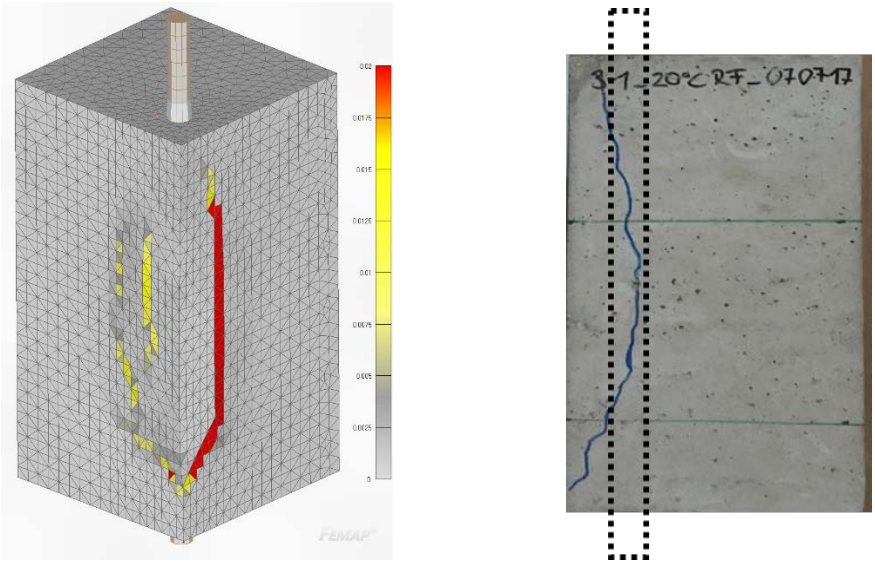

Figure 47. FE model vs experiment for the corner located rebar.

In the Table 3 all the results and depending on the C_{max}/C_{min} ratio and the covers value are showed. In the table also the names are showed so form now on the rebar position will be referred as indicated.

Name	Cmax (mm)	Cmin (mm)	Cmin/Cmax	Bond stress (MPa)
Center	72	72	1	13.72
Semicenter	72	48	2/3	13.70
Semiedge	72	36	1/2	12.24
Edge	72	24	1/3	9.73
Semicorner	48	24	1/2	9.63
Corner	24	24	1	8.24

Table 3. Bond stress for all the models for the reference case (no thermal exposure).

For the center located rebar model the stress value is the same it is for the semicenter model. In this second model the pull-out is also happening so it gives the predicted results. From the results it can also be observed that, as expected, the minimum cover is mostly defining the reduction in the strength and a major decrease is obtained when decreasing the minimum cover than when reducing the maximum. The results indicate that the bond strength can be reduced by a 40% when splitting occurs. It is also important to remark that this models have confinement so this reduction can even be greater for unconfined concrete.

3.2.4 Thermal analysis of the models

Once validated the models, the thermal analysis has been performed. For this thermal analysis the outer side of the concrete has been heated with a heating rate of 2°C/min has been applied up to the maximum temperature, after that, the models were remained at the maximum temperature to achieve a uniform thermal profile through the whole specimen and then cooled down to room temperature and finally remain the reference temperature for five hours to ensure it was completely cooled down to the 20°C. For the heating an all the thermal steps, 2 min/step have been used.

This slow heating was aimed to have the less significant effect on the thermo-mechanical damage on the concrete, so that the effect of the temperature on the concrete properties and the bond behavior could be tested.

The thermal analysis has been performed for temperatures of 300°C, 500°C and 700°C so it could be compared with available experimental tests data and also have a reference for the modelling and method performance.

3.2.4.1 Center

In the case of the center the numerical results compared to the tests can be observed in the Figure 48. It can be observed that for the 300°C the strength matches with a relative low difference that could be for example due to the experimental results variability. The same is valid both for the 500°C and 700°C models.

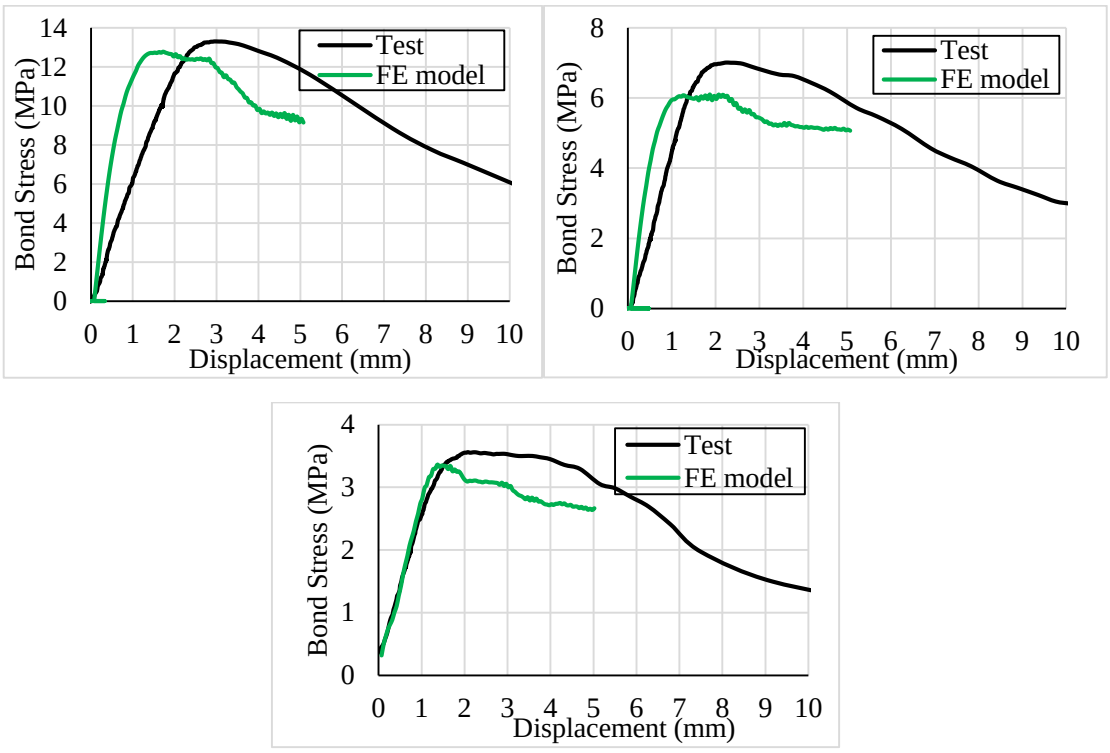

Figure 48. Center located rebar FE models vs Tests at 300°C (top left), 500°C (top right) and 700°C (bottom).

When comparing the cracking pattern of the specimens with the real models a good result is obtained. It can be seen that no splitting happens even if for the case of 700°C in which the greatest tensile strength reduction is given and therefore, splitting would be more likely to happen than in those exposed to a lower peak temperature. The results are shown in the Figure 49, Figure 50 and Figure 51.

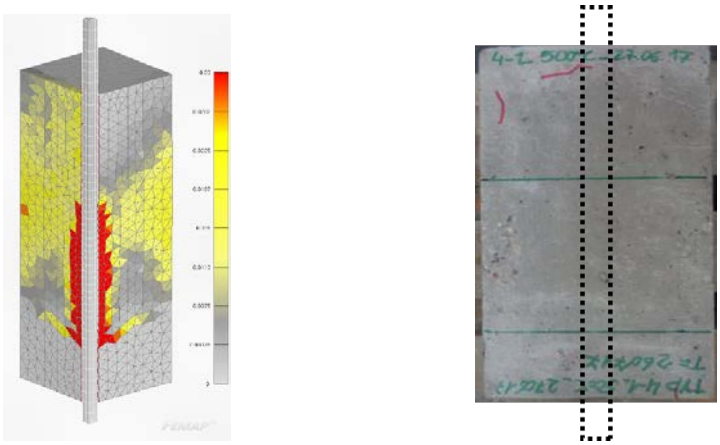

Figure 49. Center positioned rebar FE model vs experiment crack comparison at 300°C.

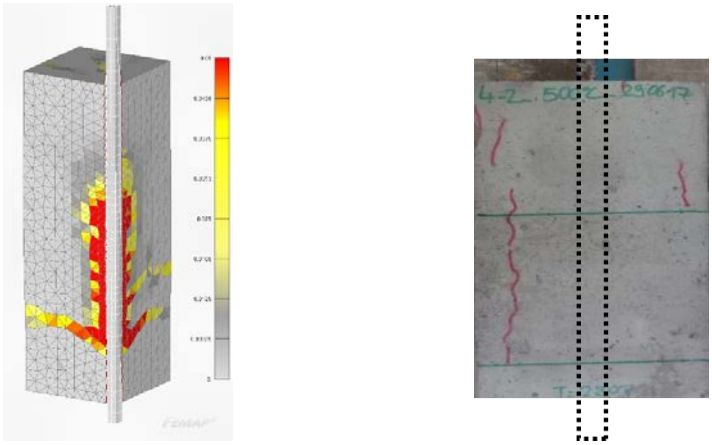

Figure 50. Center positioned rebar FE model vs experiment crack comparison at 500°C.

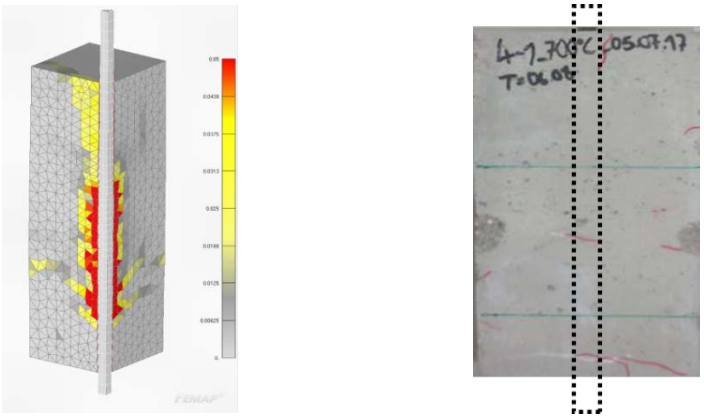

Figure 51. Center positioned rebar FE model vs experimental crack comparison at 700°C.

3.2.4.2 Edge

For the case of the edge, the results shown in the Figure 52 have been obtained. Since splitting is the failure mode, lower values for the strength are expected.

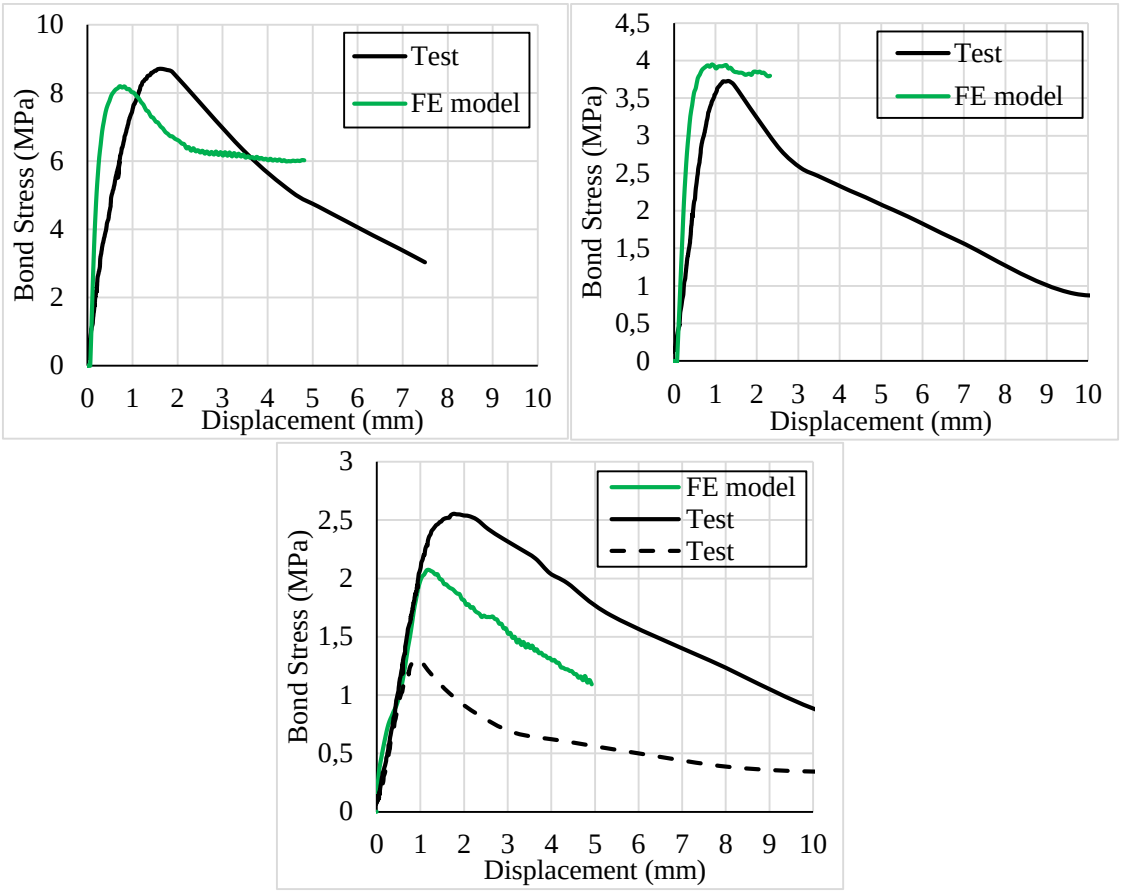

Figure 52. Edge located rebar FE models vs Tests at 300°C (top left), 500°C (top right) and 700°C (bottom).

For all the models the strength matches and for the specific case of 700°C it is the mean value of the experimental results. When comparing the cracks of the FE models with the tests in the Figure 53, Figure 54 and Figure 55 same failure mode is showed.

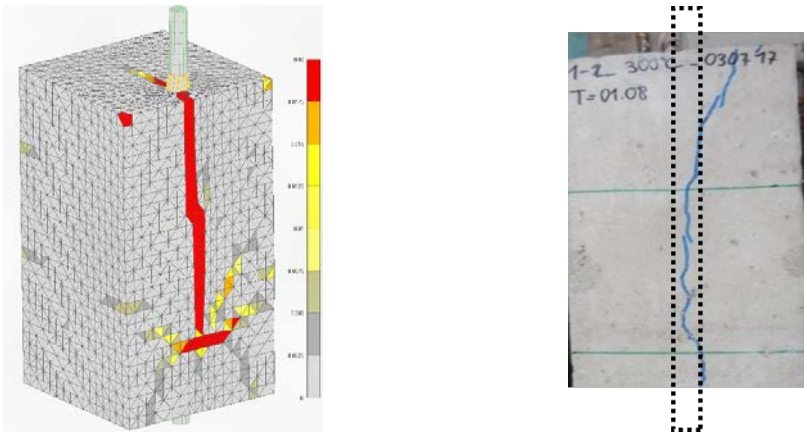

Figure 53. Edge positioned rebar FE model vs experimental crack comparison at 300°C.

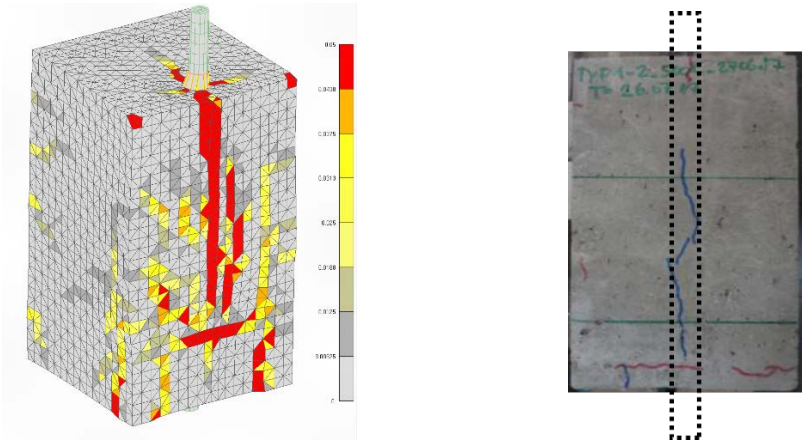

Figure 54. Edge positioned rebar FE model vs experimental crack comparison at 500°C.

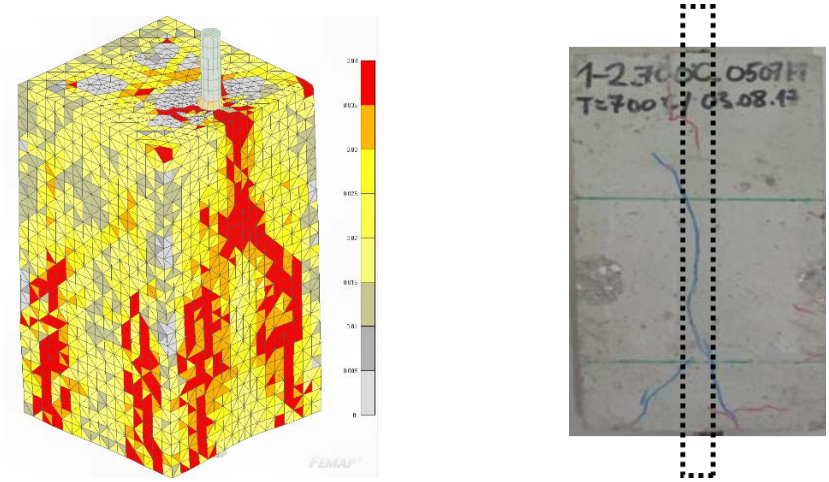

Figure 55. Edge positioned rebar FE model vs experimental crack comparison at 700°C.

For the case of 700°C the concrete is very much damaged which is caused by the thermomechanical damage. For the rest of the models we can see the same cracking pattern on both the numerical models and the experimental tests.

When evaluating the cracking pattern, it is important to consider how damaged is the model after the thermal cycle so the effect of the heating can be observed. In the experimental models the post fire cracks before loading were marked with red and the post testing cracks with blue. As this cannot be done for the models, in the Figure 56 the FE models are shown before the loading. It can be observed how for the model at 300°C almost no damage can be observed in the specimen, but for the models of 500°C and 700°C it can be observed a considerable damage where the reinforcement is located. This could be because of the steel-concrete incompatibilities leading to the start of cracking in that zone.

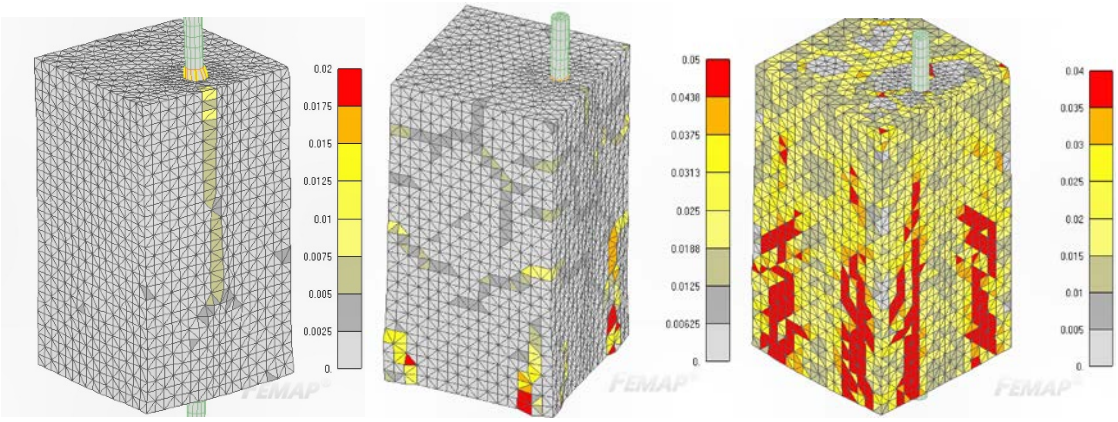

Figure 56. Post fire cracking for 300°C (left), 500°C (center) and 700°C (right).

3.2.4.3 Corner

For the corner models, the results are shown in the Figure 57. The strength presented by the models is comparable to the experimental results. In this case, as mentioned before, a higher reduction on the strength should be expected since the most critical conditions are given for the splitting failure.

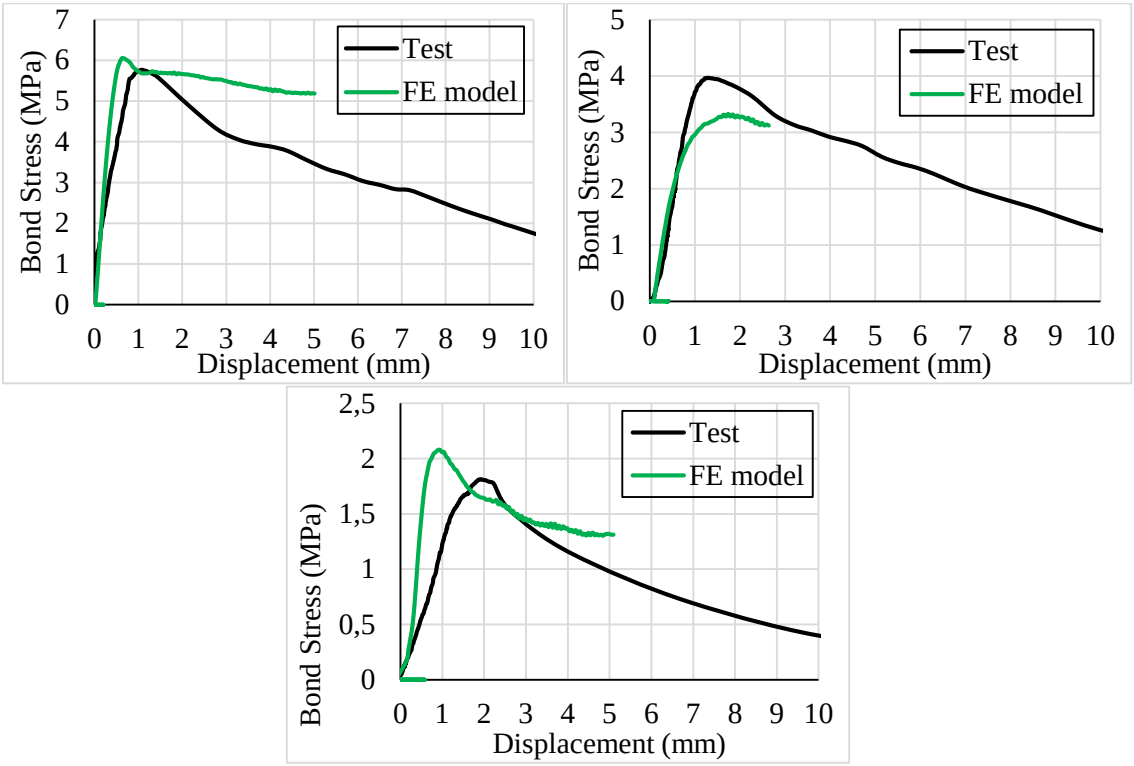

Figure 57. Corner located rebar FE models vs Tests at 300°C (top left), 500°C (top right) and 700°C (bottom).

For the failure mode the numerical model and the experimental tests match and they show similar cracks as it can be observed in the Figure 58, Figure 59 and Figure 60. As it

happens in the edge model at very high temperatures such as 700°, the thermomechanical damage on the model is very high.

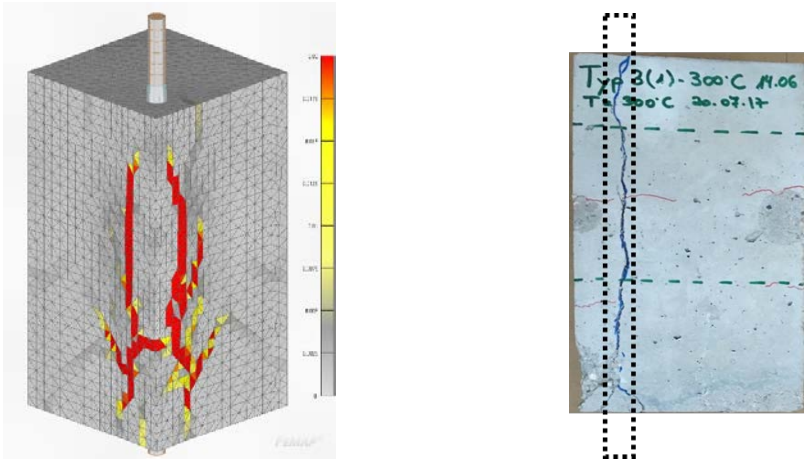

Figure 58. Corner positioned rebar FE model vs experimental crack comparison at 300°C.

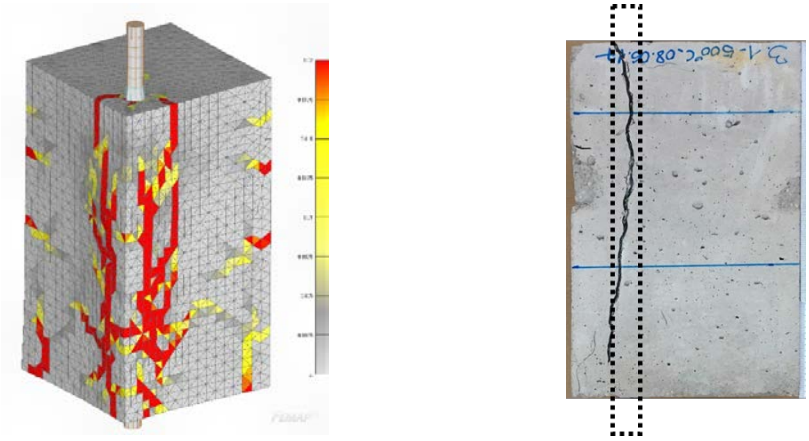

Figure 59. Corner positioned rebar FE model vs experimental crack comparison at 500°C.

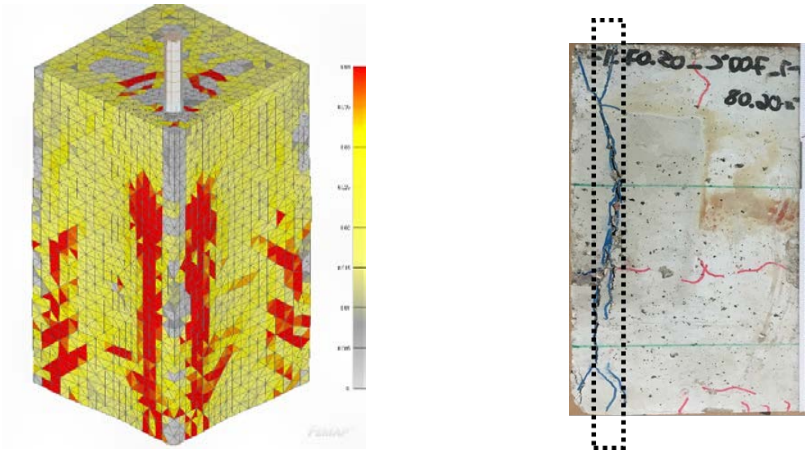

Figure 60. Corner positioned rebar FE model vs experimental crack comparison at 700°C.

3.2.4.4 Validation of the modelling approach

In the Figure 61 the reduction of the strength for all the FE models is plotted. It can be observed how for a reduction of the minimum cover a great reduction of the strength occurs. The reduction of the strength is also greater for the splitting failing specimens since the splitting is ruled by the tensile failure and the tensile strength decreases much more than the compressive strength. At temperatures about 300°C degrees for the center model almost no reduction is shown but for temperatures higher than 300°C a great reduction is presented. For the rest of the specimens the degradation is more aggressive since the beginning, but at the end the reduction is about the same, an order of the 25% the initial strength.

For the pure pull-out failure mode in the center model, the bond strength follows a degradation tendency ruled by the compressive strength reduction. Because of this reason, the reduction of the bond up to temperatures of 300°C is much smaller in comparison to the reduction for temperatures higher than this value.

For the case of the semicenter model (C_{max} = 48 mm and C_{min} = 24 mm) a transition between pull-out to splitting happens, for the room temperature the pure bond failure is shown and once heated to 300°C the splitting is the failure mode. This can clearly be observed by analyzing the reduction of the strength for 300°C. For the reference temperature since pull-out failure is also happening, no reduction is observed in the strength in comparison to the center model, but for temperatures of 300°C a greater reduction is shown.

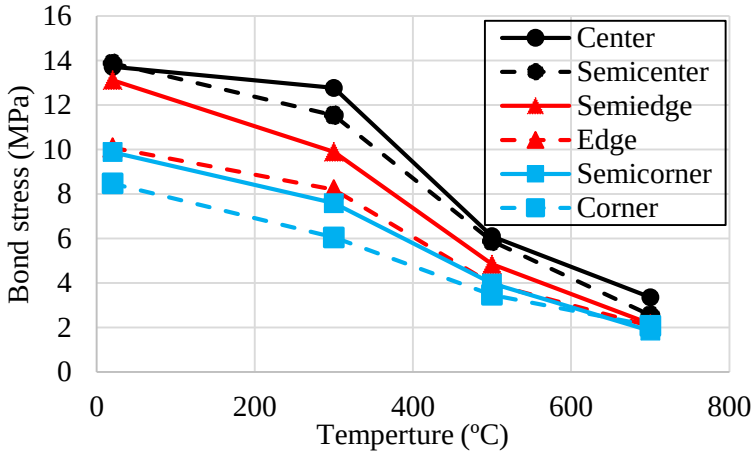

Figure 61. Numerical results on bond strength for different temperatures.

For the stiffness, it can be observed in the Figure 62 that as it happens with the bond strength, almost the greater reduction of the stiffness is happening for temperatures higher than 300°C. For the center and the edge, similar reduction is shown, but for the case of the corner a great reduction occurs in comparison to the other two models.

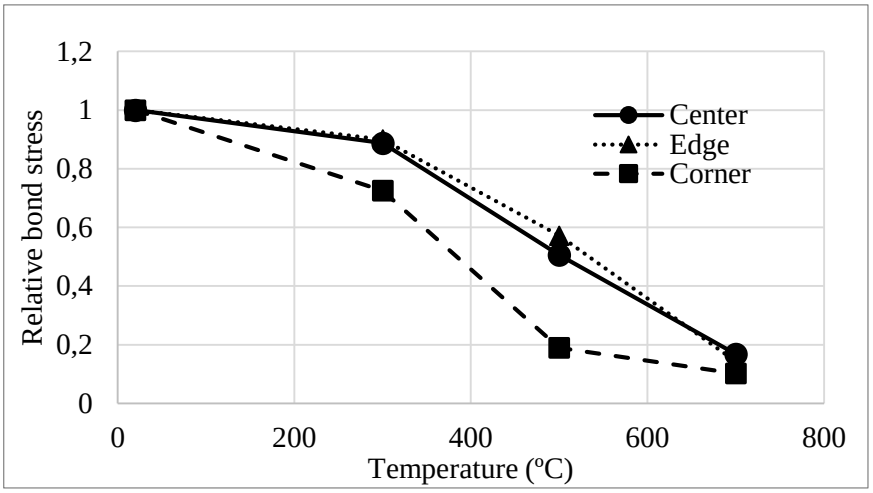

Figure 62. Relative stiffness value for center, edge and corner.

3.2.5 Bond length and bond stress development

Even if the previous results and tests in the bond stress calculation a constant stress along the length is assumed, the reality is that this stress profile is not constant. When the bond length increases, this stresses become less uniform and stress concentrations are presented in the front part of the bonded zone. Because of this real behavior, the total bond capacity is not as much as it would be if all the stresses were uniform. The fib Model Code 2010 proposes to assume a constant stress along the whole bond length and the usage of a reduction factor depending on the length for the calculation of this constant stress.

$$\tau_{red} = \tau_{ref} \left(\frac{l}{l_{ref}} \right)^{0.5} \tag{3.4}$$

Being τ_{red} the reduced bond stress, τ_{ref} the bond stress for a reference length (l_{ref}) and l the length at which the bond capacity is calculated.

By the use of the FE models, the accuracy of this assumption wants to be tested and what is the performance for higher temperatures and if further correction should be performed for higher temperatures.

For this purpose, the models have been adapted for different bond lengths, being this ones $5d_s, 8_{ds}, 10d_s, 12d_s$ and $15d_s$ so bond lengths from 80 mm to 240 have been calculated for the six different rebar positions.

3.2.5.1 Pure pull-out failure

For the pure pull-out failure the different bond lengths were tested obtaining the results shown in the Figure 63. It can be observed how even if a decrease on the bond performance is observed as there is an increase on the bond length, for this type of failure the fib Model Code 2010 does not match. For higher temperatures even if there is a

decrease in the bond stress as there is an increase on the length, it cannot be assumed to be a good approximation to determine the behavior.

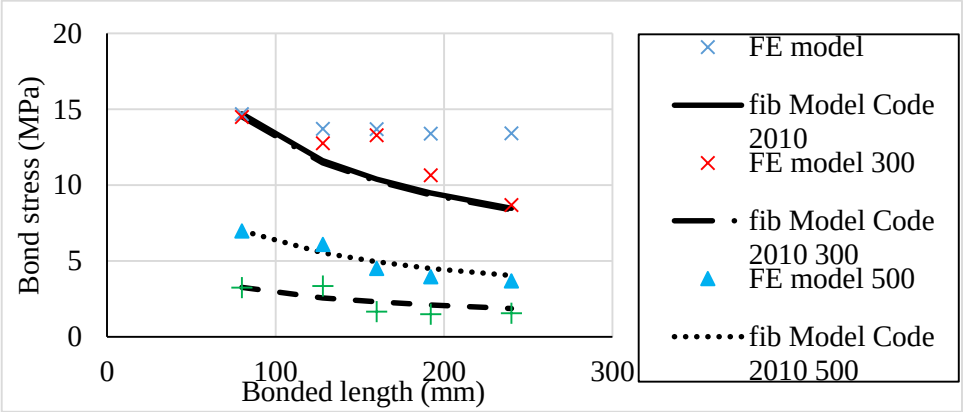

Figure 63. Bond stress for different bond lengths for the center located rebar FE model and the fib Model Code 2010 approximation.

For the case of the semicenter located rebar (Cmin = 48 mm) the results obtained can be seen in the Figure 64. In this case, even if for te reference temperature splitting is not happening, it fits better the approximation provided by the fib Model Code 2010. For the case of 300°C since the splitting is happening it fits better the approximation.

When splitting starts to happen is can be seen that the results fit the approximation much better and starts becoming a valid approximation, even for high temperatures.

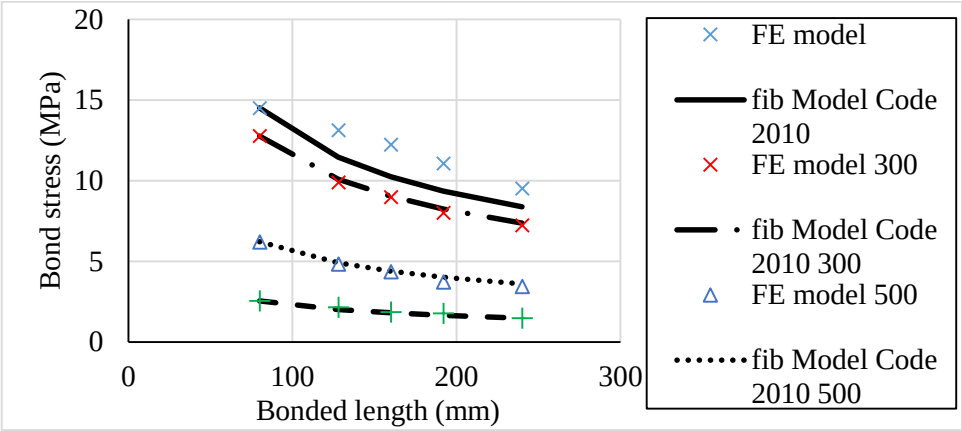

Figure 64. Bond stress for different bond lengths for the semicenter located rebar FE model and the fib Model Code 2010 approximation.

3.2.5.2 Splitting failure

When splitting is happening, this approach proposed by the fib Model Code 2010 is aimed to be tested. The results for the rebar located at the edge have been plotted in the Figure 65. It can be observed that in this case it perfectly follows the fib Model Code 2010 proposal and it also does for the different temperatures. This results verify that the approach can also be considered for models at high temperatures. For other applications like fire in which the concrete could be very much damaged, it cannot be clearly defined

if this approach will be accurate since other factor are involved and probably the damage on the concrete would involve a greater reduction.

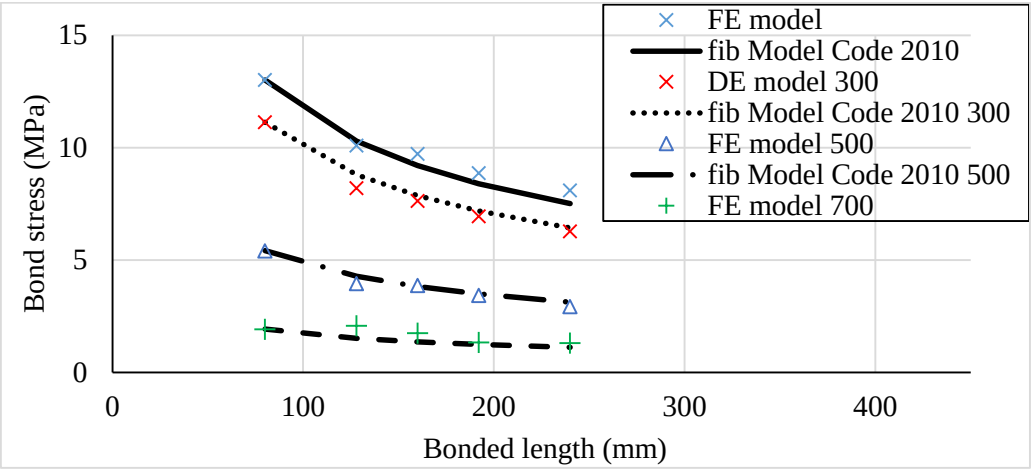

Figure 65. Bond stress for different bond lengths at different temperatures in the edge located rebar model.

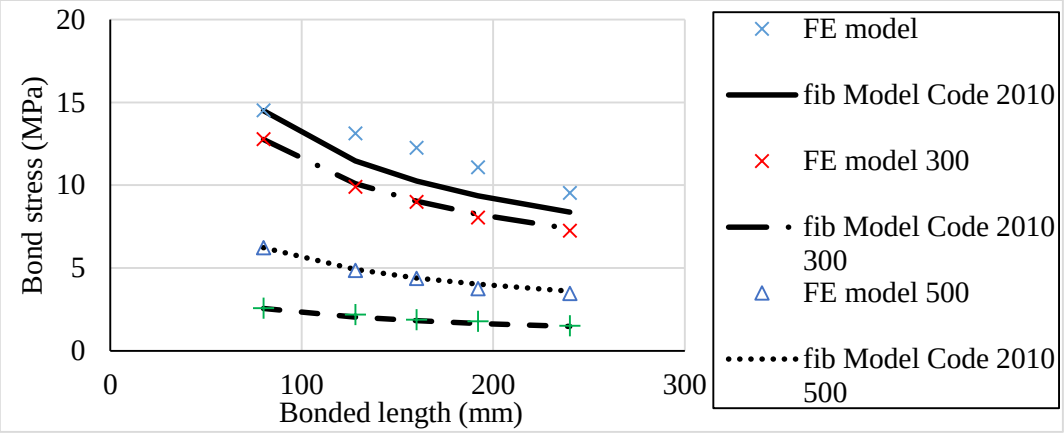

Figure 66. Bond stress for different bond lengths at different temperatures in the semiedge located rebar model.

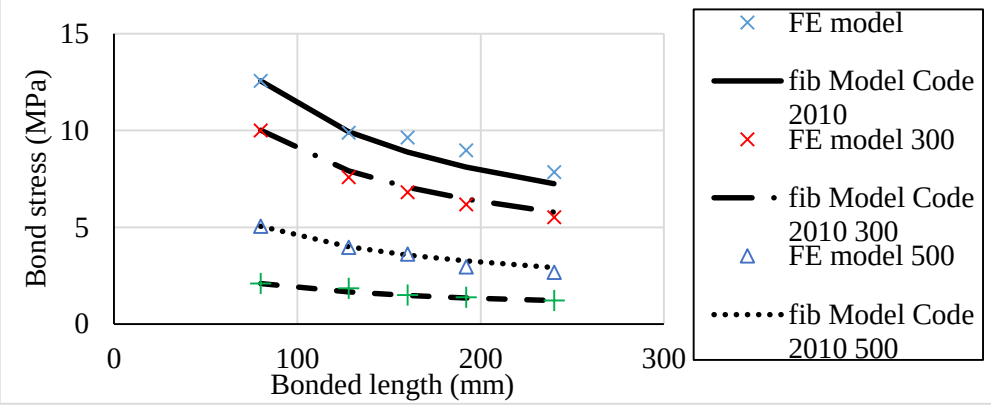

Figure 67. Bond stress for different bond lengths at different temperatures in the semicorner located rebar model.

It can also be observed that as there is a reduction on the cover, the results start to fit the approximation for the reference temperature more accurately. This was previously observed when comparing the pull-out failure, even if it was confirmed that the approximation is not valid for that type of failure. In this case for the model of the semiedge located rebar (Figure 66) in which a cover of 36 mm is set, does not follow the fib Model Code 2010 approximation as much as the other models with the rebar located in the edge and semicorner for which the cover is 24 mm.

In all the models for higher temperatures the Code proposal seems to be a good approximation.

4 Conclusions

In this numerical study, the bond behavior after exposure to elevated temperatures has been performed. For this purpose, different finite element models have been modelled based on previous studies performed before in the Stuttgart University by Bosnjak et al. (2017). For this study different pull-out test were performed for different rebar positions at different temperatures. For the validation of the model this study has been reproduced numerically for validation.

After the validation of the models for the reference temperature, a slow heating has been applied on the concrete models sides to achieve a low temperature gradient. Therefore, the thermomechanical damage on the concrete was minimized to be able to analyze the decrease of the bond only due to the degradation of the concrete when it reaches high temperatures. In this analysis only the decrease of the properties due to the temperature are taken into account, so the after heating model will be completely determined by the maximum temperature reached during the heating.

When compared to the experimental available data, the models show a good behavior for the bond modelling. The results match both in the strength and the failure mode. It was also found out that the compressive strength has a great influence in the pure bond failure and for temperatures up to 300°C almost no decrease on the strength was presented. When splitting is happening, the tensile strength reduction is more critical when determining the strength. Because of this reason, the models having a splitting type failure have a greater decrease on the strength and it is also presented at relatively low temperatures.

It was also observed that the minimum cover influences much more than the maximum cover and once the minimum cover of 24 mm was reached, when the maximum cover was reduced from 72 mm to 24 mm the strength barely decreased.

Further analysis could be proposed on behalf of the usage of different concrete types such as fiber reinforced concrete.

It was also observed that for some specimens a transition from pull-out failure to splitting can happen when heating, decreasing greatly the performance at high temperatures in comparison to these models for which the pure bond failure happens for the whole range of temperatures. Further analysis of the effect of the cover and the failure mode transition is proposed to determine the effect of the cover in the failure mode at high temperatures.

To determine the bond stress depending on the bond length assuming a constant value for the stress development as indicated in the fib Model Code 2010, the same models were altered changing the bond length. It was tested both for the pure pull-out failure mode and the splitting failure affirming that for the pure pull-out specimens even if the bond stress decreasing tendency also was shown, it did not follow the curve proposed by the code. For the splitting failure the results have been much more satisfactory determining it really is a good approximation for this type of failure. It has also been observed that the less the cover, the closer the values will be to this proposal. When tested for high temperatures it was observed that this fib Model Code 2010 proposal is also valid without any need of adaptation.

To conclude it can be affirmed that the temperature dependent microplane model shows a realistic behavior when testing the post-heating behavior of the concrete. Through the validation of the numerical approach against experimental results it is shown that the model is able to realistically predict the bond capacity in the case of both bond and splitting failure. Furthermore, it is found that the model can capture the thermal degradation of concrete and its effect on the degradation of bond, without any explicit definition of bond degradation within the thermomechanical model for concrete.

Further analysis is proposed to determine the bond reduction with models for which a fire ISO standard curve is applied to the comparison of the results and how greater the damage is when fire is applied. It is also proposed to analyze the behavior of different concrete types in the same application. The loaded while heating after cooling analysis shows also as a good research line to determine if there is any difference in the bond properties when load has been applied.

5 Bibliography

American Concrete Institute, & Bundesanstalt für Materialprüfung (Germany) (Eds.). (1972). *Concrete for nuclear reactors.* Detroit: American Concrete Institute.

Anderberg, Y., & Forsén, N. E. (1982). Fire Resistance of Concrete Structures.

Balász, G. L., & Eligehausen, R. (1991). Bond between concrete and steel.

Bažant, Z. P., & Kaplan, M. F. (1996). *Concrete at high temperatures: material properties and mathematical models*. Harlow: Longman.

Bosnjak, J., Sharma, A., & Bessert, S. (2017). Bond performance of reinforcement in concrete after exposure to elevated temperatures (pp. 850–861). Stuttgart.

Calmeiro dos Santos, C., & Joao, P. R. (2015, April). EXPERIMENTAL TESTING ON THE RESIDUAL MECHANICAL PROPERTIES OF ORDINARY CONCRETES AFTER FIRE

Christiaanse, A., Langhorst, A., & Gerriste, A. (1972). *Discussion of fire resistance of lightweight concrete and spalling*. Dutch Society of Engineers.

Cruz, C. R., & Gillen, M. (1980). Thermal expansion of Portland cement paste, mortar and concrete at high temperatures.

D. J. Naus. (2005). The Effect of Elevated Temperature on Concrete | Concrete | Strength Of Materials.

Diederichs, U., & Schneider, U. (1981). Bond strength at high temperatures. *Magazine of Concrete Research*, *33*(115), 75–84.

EN 1992-1-2: Eurocode 2: Design of concrete structures - Part 1-2: General rules - Structural fire design : European Committee for Standardisation. (2004).

F. Sciarretta, F. Haider, & M. Korsunsky. (2015). First Evaluation of the Structural Performance of Traditional Brickwork after Standard Fire Exposure.

Ferguson, P. M., & Thompson, J. N. (1965). Development Length for Large High Strength Reinforcing Bars. *Journal Proceedings*, *62*(1), 71–94.

Hager, I. (2013). *Behaviour of cement concrete at high temperature* (Vol. 61).

Hager, I. (2004). Comportement a haute temperature des betons a haute performance - evolution des principales proprietes mecaniques.

Hager, I., & Mróz, K. (2015). AN OVERVIEW OF CONCRETE MODULUS OF ELASTICITY EVOLUTION WITH TEMPERATURE AND COMMENTS TO EUROPEAN CODE PROVISIONS.

Hossain, K. M. A. (2018). Bond Strength of GFRP Bars Embedded in Engineered Cementitious Composite using RILEM Beam Testing. *International Journal of Concrete Structures and Materials*, *12*(1), 6.

H.S. Davis. (1972). N - Reactor Shielding. *Special Publication, 34*.

Irving, J. (1975). *The effect of elevated temperatures on concrete and concrete structures*. Wexham Springs: Fédération Internationale de la Précontrainte.

J. E. Sullivan, P., A. Khoury, G., & N. Grainger, B. (1986). *Strain of concrete during first cooling from 600°C under load* (Vol. 38).

J. Piasta, Z. Sawicz, & L. Rudzinski. (1984). Changes in the structure of hardened cement paste due to high temperature.

J. Stabler. (2000). *Computational modelling of thermomechanical damage and plasticity in concrete*. The University of Queensland, Australia.

Kordina, K., Meyer-Ottens, C., & Richter, E. (1999). *Beton-Brandschutz-Handbuch* (2., überarb. Aufl. edition). Düsseldorf: Bau + Technik.

Lee, J., Xi, Y., Willam, K., & Jung, Y. (2009). A multiscale model for modulus of elasticity of concrete at high temperatures. *Cement and Concrete Research*, *39*(9), 754–762.

Lee, J., Xi, Y., & William, K. (2008). Properties of Concrete After High-Temperature Heating and Cooling. *ACI Materials Journal*, *105*(4).

Lublóy, É., & György, L. B. (2014). Temperature effects on bond between concrete and reinforcing steel

Malhotra, H. L. (1956). The effect of temperature on the compressive strength of concrete. *Magazine of Concrete Research*, *8*(23), 85–94.

Meyer-Ottens, C. (1974). *Abplatzversuche an Prüfkörpern aus Beton, Stahlbeton und Spannbeton bei verschiedenen Temperaturbeanspruchungen*.

Milon, K., Howlader, M., Rashid, H., Mallick, D., & Haque, T. (2012). EFFECTS OF AGGREGATE TYPES ON THERMAL PROPERTIES OF CONCRETE. *ARPN Journal of Engineering and Applied Sciences*, *VOL. 7, NO. 7*.

Mousa, M. I. (2016). Effect of bond loss of tension reinforcement on the flexural behaviour of reinforced concrete beams. *HBRC Journal*, *12*(3), 235–241.

Odelson, J. B., Kerr, E. A., & Vichit-Vadakan, W. (2007). Young's modulus of cement paste at elevated temperatures. *Cement and Concrete Research*, *37*(2), 258–263.

Ožbolt, J., Li, Y., & Kožar, I. (2001). Microplane model for concrete with relaxed kinematic constraint. *International Journal of Solids and Structures*, *38*(16), 2683–2711.

Park, R., & Paulay, T. (1975). *Reinforced Concrete Structures* (Edición: 1). New York: Wiley.

Periskic, G. (2009). *Entwicklung eines 3D thermo-hygro-mechanischen Modells für Beton unter Brandbeanspruchung und Anwendung auf Befestigungen unter Zuglasten*.

Phan, L. T., & Carino, N. J. (2001). Mechanical Properties of High-Strength Concrete at Elevated Temperatures | NIST. *NIST Interagency/Internal Report (NISTIR) - 6726*.

Pimienta, P., Cruz Alonso, M., McNamee, R., & Mindeguia, J.-C. (2017). *Behaviour of high-performance concrete at high temperatures: some highlights* (Vol. 2).

Rehm, G. (1961). *The basic principles of the bond between steel and concrete*. Cement and Concrete Association.

Schneider, U. (1973). *Zur Kinetik festigkeitsmindernder Reaktionen in Normalbetonen bei hohen Temperaturen.* Braunschweig.

Sharma, A., Bošnjak, J., Ožbolt, J., & Hofmann, J. (2016). Numerical modeling of reinforcement pull-out and cover splitting in fire-exposed beam-end specimens. *Engineering Structures*, *111*, 217–232.

Sheffield, U. of. (n.d.). LITS+Damage: Load Induced Thermal Strain and Damag - Projects - Multi-axial compression of concrete - Research Activities - Construction Innovation - The University of Sheffield. Retrieved September 10, 2018, from https://www.sheffield.ac.uk/ci/research/mac2t/res/lits

Tastani, S., Eleftheriou, T., & Pantazopoulou, S. (2013). *Bond of reinforcing bars embedded in ECC*.

Varona, B., Baeza, J., Ivorra, S., & Bru, D. (2011). Experimental analysis of the loss of bond between rebars and concrete exposed to high temperatures.

Youssef, M. A., & Moftah, M. (2007). General stress–strain relationship for concrete at elevated temperatures. *Engineering Structures*, *29*(10), 2618–2634.

Zhang, B., & Bicanic, N. (2002). *Residual fracture toughness of normal- and high-strength gravel concrete after heating to 600°C* (Vol. 99).